Phycologia
2021, Volume 60, Issue 4, Pages 332-353
https://doi.org/10.1080/00318884.2021.1930796
https://archimer.ifremer.fr/doc/00705/81667/

Cyst-theca relationships of *Spiniferites bentorii*, S. *hyperacanthus*, *S. ramosus*, *S. scabratus* and molecular phylogenetics of *Spiniferites* and *Tectatodinium* (Gonyaulacales, Dinophyceae)

Gu Haifeng [1, *], Huo Kai [1], Krock Bernd [2], Bilien Gwenael [3], Pospelova Vera [4], Li Zhen [5], Carbonell-Moore Consuelo [6], Morquecho Lourdes [7], Ninčević Živana [8], Mertens Kenneth [3, *]

[1] Department of Marine Biology and Ecology, Third Institute of Oceanography, Ministry of Natural Resources, Xiamen, Fujian, 361005, China
[2] Department of Ecological Chemistry, Alfred Wegener Institute for Polar and Marine Research, Am Handelshafen 12, Bremerhaven, D-27570, Germany
[3] Station de Biologie Marine, Ifremer, LITTORAL, Place de la Croix, BP40537, 29900 Concarneau CEDEX, France
[4] Department of Earth and Environmental Sciences, University of Minnesota, 116 Church Street SE, Minneapolis, Minnesota 55455, USA
[5] Department of Earth, Ocean and Atmospheric Sciences, University of British Columbia, 329 West Mall, Vancouver, BC, V6T 1Z4, Canada
[6] Department of Botany and Plant Pathology, College of Agricultural Sciences, Oregon State University, 2082 Cordley Hall, Corvallis, Oregon 97331-2902, USA
[7] Department of Environmental Planning and Conservation, Centro de Investigaciones Biológicas del Noroeste (CIBNOR), Av. IPN #195, Playa Palo de Sta. Rita Sur, La Paz, Baja California Sur, 23096, Mexico
[8] Laboratory of Plankton and Shellfish Toxicity, Institute of Oceanography and Fisheries (IOF), Šetalište I. Meštrovića 63, Split, 21000, Croatia

* Corresponding authors : Haifeng Gu, email address : guhaifeng@tio.org.cn ; Kenneth Mertens, email address : kenneth.mertens@ifremer.fr

Abstract :

It is well known that modern resting cysts with morphologies matching those of species of the fossil genus Spiniferites germinate into motile cells of the genus Gonyaulax. Different Spiniferites species have been connected to a single Gonyaulax species, raising the question of whether they are over-classified. Through germination experiments of cysts with the morphological features of four species of Spiniferites, viz. S. bentorii, S. hyperacanthus, S. ramosus and S. scabratus, we established cyst-theca relationships. Cysts with the morphology of S. bentorii gave rise to vegetative, motile cells of Gonyaulax nezaniae sp. nov., which is characterized by two stout antapical spines. Cysts with S. hyperacanthus and S. ramosus morphologies germinated into Gonyaulax whaseongensis and G. spinifera, respectively. Cysts with S. scabratus morphology lacked a ventral pore and were attributed to Gonyaulax cf. spinifera. Gene sequences for SSU, LSU and/or ITS-5.8S rRNA were obtained from these four species, and from cysts with the morphology of Spiniferites belerius, S. mirabilis, S. lazus, Spiniferites cf. bentorii and

Tectatodinium pellitum. The maximum likelihood and Bayesian inference analyses based on LSU and SSU rRNA gene sequences revealed that cysts assignable to Spiniferites formed a polyphyletic group, intermingled with Tectatodinium, Bitectatodinium, Ataxiodinium and Impagidinium, whereas Gonyaulax species appeared as monophyletic. From our results we inferred the phylogenetic positions of S. bentorii, S. mirabilis, S. lazus, S. scabratus, Tectatodinium pellitum and Gonyaulax digitale for the first time, supporting the idea that Spiniferites species are not over-classified and each of them may correspond to different Gonyaulax species.

Keywords : Dinoflagellates, Gonyaulax nezaniae, Gonyaulax spinifera, Tectatodinium pellitum

INTRODUCTION

The International Code of Nomenclature for algae, fungi and plants (ICN; Turland *et al.* 2018) permits the use of different names for dinoflagellate species with fossil types (generally a cyst; e.g. Head *et al.* 2016) and extant species with non-fossil types (usually based on motile cells) even when the fossil and modern forms are considered conspecific (Turland *et al.* 2018, Art. 11.7 and 11.8). Classic examples of the use of two names for taxa often considered the same species are found in the fossil genus *Spiniferites* Mantell and the extant genus *Gonyaulax* Diesing. The relationship between *Spiniferites* and *Gonyaulax* was first established through germination of a living cyst with the morphological features of *Hystrichosphaera bentorii* M. Rossignol [now known as *Spiniferites bentorii* (M. Rossignol) D. Wall & B. Dale], from which a motile cell emerged. This cell was identified as *G. digitalis* (C.H.G. Pouchet) Kofoid (Wall & Dale 1966). *Spiniferites* cysts display the tabulation formula 2pr, 4′, 6″, 6c, 5–6s, 6‴, 1p, 1⁗ and possess gonal and/or intergonal processes (the former are always trifurcate and the latter are always bifurcate), sutural ridges or septa connecting their bases, and a precingular archeopyle formed by the loss of plate 3″ (Mertens & Carbonell-Moore 2018). 2pr was first introduced by Lewis *et al.* (1999) and refers to the presence of an apical pore complex and a ventral pore on the epitheca. One hundred and six species of *Spiniferites* are currently accepted (Williams *et al.* 2017). Key features to differentiate *Spiniferites* species include size and shape of central body, number, location and shape of processes, the presence or absence of an apical boss, wall surface ornamentations, and cingulum displacement. However, the morphology of these species may intergrade,

which complicates their identification (Mertens *et al.* 2018b). The type species of *Spiniferites*, *S. ramosus* (Ehrenberg) Mantell was described from the Senonian (Upper Cretaceous; Sarjeant 1970).

Only 13 *Spiniferites* species have been reported from modern material (Zonneveld *et al.* 2013; Price & Pospelova 2014; Mertens & Carbonell-Moore 2018). The cyst-theca relationship of some *Spiniferites* species has been established, e.g. *S. bentorii* and *S. ramosus* have been connected to *Gonyaulax digitalis* and *G. spinifera* (Claparède & J. Lachmann) Diesing, respectively (Wall & Dale 1967, 1970). However, *Spiniferites mirabilis* (M. Rossignol) Matsuoka, *S. elongatus* P.C. Reid and *S. membranaceus* (M. Rossignol) Sarjeant have also been connected to *G. spinifera* (Wall & Dale 1968; Dale 1976), although later *S. membranaceus* and *S. elongatus* were transferred to *Gonyaulax* as the two independent species *G. membranacea* (M. Rossignol) Ellegaard, Daugbjerg, Rochon, Jane Lewis & I. Harding and *G. elongata* (P.C. Reid) Ellegaard, Daugbjerg, Rochon, Jane Lewis & I. Harding, respectively (Ellegaard *et al.* 2003). Several other cyst-defined genera were reported to produce motile cells which were similar to *Gonyaulax spinifera*, including *Nematosphaeropsis balcombiana* Deflandre & Cookson, *Ataxiodinium choanum* P.C. Reid and *Tectatodinium pellitum* D. Wall (Wall & Dale 1968; Morquecho *et al.* 2009). Later, *Bitectatodinium tepikiense* G.J. Wilson was also connected to *Gonyaulax digitalis* (Lewis *et al.* 2001), which casts doubt on the assignment of *G. digitalis* as the parent theca of *S. bentorii*-like cysts (Wall 1965). The assignment of numerous fossil-based species to a single extant species (*G. spinifera*) would suggest that the fossil-based species are over-classified.

The non-fossil genus *Gonyaulax* was established with *G. spinifera* as the type species (Diesing 1866). However, the cell morphology of *Gonyaulax* is rather conservative, and three morphologically similar species have been placed in the *Gonyaulax spinifera* group, namely *G. spinifera*, *G. digitalis* and *G. diegensis* Kofoid (Kofoid 1911). The tabulation of the genus *Gonyaulax* was interpreted as Po, 3′, 2a, 6″, 6c, 4–8s, 5‴, 1p, 1⁗ (Dodge 1989), but this was later reinterpreted as 2pr, *4′, 6″, 6c, ?s, *6‴, 1p, 1⁗ (Lewis *et al.* 1999; Carbonell-Moore & Mertens 2019). Lewis *et al*. (1999) interpreted the third apical plate as Cv (Taylor-Evitt notation), thus the two Kofoidean intercalary plates were designated as the third and fourth apical homologues (*3′, *4′), as previously proposed by Fensome *et al.* (1993).

Heterospory (one species producing several cyst types) has been proposed for the genus *Gonyaulax* (Wall & Dale 1968, p. 270). This was demonstrated for *Gonyaulax baltica* Ellegaard, Jane Lewis & I. Harding, which was related to two cyst types: one resembling *Spiniferites bulloideus* (Deflandre & Cookson) Sarjeant and another like *Impagidinium caspienense* F. Marret (Ellegaard *et al.* 2002; Mertens *et al.* 2018a). In addition, crossed strains of *Gonyaulax spinifera*-like cells produced cysts similar to both *Spiniferites ramosus* and *Nematosphaeropsis labyrinthus* (Ostenfeld) P.C. Reid, and the expression of a particular phenotype was attributed to the specific salinity conditions (Rochon *et al.* 2009). However, a number of *Gonyaulax* species have been shown not to be heterosporous: *G. elongata*, *G. membranacea* and *G. ellegaardiae* K.N. Mertens, H. Aydin, Y. Takano, A. Yamaguchi & Matsuoka were proposed to be the respective motile stages of cysts resembling *Spiniferites elongatus, S. membranaceus* and *S. pachydermus* (M. Rossignol) P.C. Reid, with differences

in morphology of both cyst and motile stage as well as in LSU rRNA gene sequence (Ellegaard *et al.* 2003; Mertens *et al.* 2015).

Whether the extant material examined herein represents the same species that we know from fossilized cysts, formed tens or hundreds of thousands of years ago, is debatable. However, we assume a close relatedness between fossil and modern species producing cysts with very similar morphologies. To keep the text simple, in the following we refer to the cysts of our modern material that match the morphology of fossilized cysts by the names used for the corresponding fossil species.

It is of note that some species of *Gonyaulax* can produce yessotoxin (YTX), a marine polyether toxin that was first isolated from the scallop *Mizuhopecten yessoensis* Jay (Murata *et al.* 1987). To date, 92 variants of YTX-like ladder shape polyketide toxins have been reported, but most of them have not yet been structurally characterized (Miles *et al.* 2005). Therefore, they are commonly named yessotoxins (YTXs) and adriatoxins (ATX) (Ciminiello *et al*. 1998; Domínguez *et al.* 2010). Some strains identified as *Gonyaulax spinifera* were reported to produce yessotoxins while others did not (Riccardi *et al.* 2009; Chikwililwa *et al.* 2019; Pitcher *et al.* 2019), highlighting the importance of precise identification. In fact, the strain identified as *G. spinifera* producing homoYTX and 45-hydroxyYTX in South Africa (Pitcher *et al.* 2019) was probably *G. membranacea* instead, as inferred from the molecular sequences presented. A strain identified as *Gonyaulax taylorii* Carbonell-Moore was reported to produce YTXs but unfortunately a molecular sequence was not provided (Álvarez *et al.* 2016).

Cyst-theca relationships of *Spiniferites ramosus*, *S. bentorii*, *S. mirabilis* and *Tectatodinium pellitum* have been established (Wall 1965; Lewis *et al.* 1999; Morquecho *et al.* 2009), but since no molecular sequences were obtained, the taxonomic identity of the motile stage needs reassessing. On the other hand, cyst-theca relationships of *S. hyperacanthus* (Deflandre & Cookson) Cookson & Eisenack, *S. lazus* P.C. Reid and *S. scabratus* (D. Wall) Sarjeant have not been examined yet and their molecular sequences are not available. *Spiniferites* and related genera appear as para- or polyphyletic in molecular phylogenies based on small subunit ribosomal RNA (SSU rRNA) and large subunit ribosomal RNA (LSU rRNA) gene sequences (Ellegaard *et al.* 2018; Mertens *et al.* 2018a), suggesting that taxonomic revisions are needed. To address the question of whether *Spiniferites* and related genera are over-classified, we isolated single cysts worldwide and performed germination experiment to obtain SSU, LSU and/or ITS–5.8S rRNA gene sequences of motile cells. Both cyst and theca morphologies were examined in detail with light microscopy (LM) and scanning electron microscopy (SEM) of selected strains, and molecular phylogeny was inferred based on LSU and SSU rRNA gene sequences. In addition, strains of *S. hyperacanthus* and *S. ramosus* were examined for yessotoxin production by liquid chromatography coupled with tandem mass spectrometry (LC-MS/MS).

MATERIAL AND METHODS

Sample collection and treatment

To isolate cysts, sediment sampling was done using an Ekman grab in coastal waters of China, Diana Lagoon (Corsica, France), Baie de Vilaine (France), Pantan (Croatia), and a

Petite Ponar grab in Saanich Inlet (western Canada), between 2011 and 2020 (Table 1). In addition, surficial sediment was collected by a diver at a lagoon located at Isla San José in the Gulf of California on 13 April, 2014. The island is at the northern end of Bahía de La Paz (Table 1). For most samples, the top 2 cm of sediment were collected. The samples were stored in the dark at 4°C until further treatment. Approximately 5 g of wet sediment was mixed with 20 ml of filtered seawater and stirred vigorously to dislodge detrital particles. The settled material was subsequently sieved through 120 µm and 10 µm mesh and washed and collected with filtered seawater. Single cysts were isolated from residues using a micropipette with an inverted Eclipse TS100 (Nikon, Tokyo, Japan) microscope and incubated in small containers with f/2-Si medium (Guillard & Ryther 1962) at 20°C, and 90 µmol m^{-2} s^{-1} under a 12:12 h light:dark cycle (hereafter called standard culture conditions). A water sample was collected in Concarneau Bay, France, on 12 February 2008, from which a motile cell of *Gonyaulax digitalis* was isolated (Fig. S1).

Morphological study of thecate stages and cysts

Living cells and cysts of all strains (for which a culture is available) or isolates (without a culture) listed in Table 1 were examined and photographed using a Zeiss Axio Imager light microscope (Zeiss, Göttingen, Germany) equipped with a Zeiss Axiocam HRc digital camera. Cell and cyst size was measured on LM images.

For scanning electron microscopy (SEM), mid-exponential batch cultures of selected strains were concentrated with a Universal 320 R centrifuge (Hettich-Zentrifugen, Tuttlingen, Germany) at 850 *g* for 10 min at room temperature. Cells were fixed with 2.5%

glutaraldehyde for 3 h at 8°C, and rinsed twice with deionized water. The supernatant was removed and the settled cells were transferred to a coverslip coated with poly-L-lysine (molecular weight 70,000–150,000). The cells attached to the coverslip were rinsed twice in deionized water and dehydrated through a graded ethanol series (10%, 30%, 50%, 70%, 90% and 3× in 100%, 10 min at each step), critical-point-dried using a K850 Critical-Point Dryer (Quorum/Emitech, West Sussex, UK), sputter-coated with gold using a Hitachi JFC-1600 sputter-coater (Hitachi, Japan), and examined with a Zeiss Sigma FE (Zeiss, Oberkochen, Germany) scanning electron microscope at Xiamen University, China.

For SEM of cultures obtained from cysts with the morphologies of *Spiniferites bentorii* and *S. belerius* P.C. Reid, single specimens were isolated using a micropipette on a IX70 (Olympus) inverted microscope. The cells were deposited on polycarbonate membrane filters (GTTP Isopore, 0.22 μm pore size; Millipore, Billerica, MA, USA), which were rinsed with distilled water. The filters were processed following the methods described in Chomérat & Couté (2008). They were dehydrated in a graded series of ethanol baths (15%–100%), critical-point-dried, attached to a stub using double-sided adhesive tape and coated with gold. The stubs were examined at the Station of Marine Biology in Concarneau, France, using a Sigma 300 Gemini (Zeiss, Oberkochen, Germany) field-emission SEM equipped with both a conventional Everhart-Thornley and an in-lens secondary electron detector at 1.5 kV. Tabulation labelling follows the Kofoidean system (Kofoid 1909, 1911). Sulcal plate labelling follows Balech (1980).

PCR amplifications and sequencing

Single cells or cysts were isolated and washed several times with sterile distilled water. They were broken by applying gentle force on the coverslip and used for templates. Various regions of the ribosomal RNA (rRNA) genes including the SSU, partial LSU (D1–D6) and ITS1–5.8S–ITS2 were amplified using primer pairs specified previously and following standard protocols (Luo *et al.* 2019). The SSU rRNA gene of *G. digitalis* collected in Concarneau Bay was sequenced following the procedures described in Wang *et al*. (2019). Newly obtained sequences were deposited in GenBank with accession numbers MW775678 to MW775720, MW795366 and MW793450.

Sequence alignment and phylogenetic analyses

Newly obtained LSU rRNA (*c*. 1300 bp) and SSU rRNA (*c.* 1700 bp) gene sequences were aligned with sequences of *Gonyaulax* species and related taxa available in GenBank. Sequences were aligned using MAFFT v7.110 (Katoh & Standley 2013) online program (http://mafft.cbrc.jp/alignment/server/) with default settings. Alignments were manually checked with BioEdit v7.0.5 (Hall 1999). The final alignment consisted of 1370 (LSU) and 1853 (SSU) base pairs including introduced gaps. For Bayesian inference (BI), the program jModelTest (Posada 2008) was used to select the most appropriate model of molecular evolution with Akaike Information Criterion (AIC). Bayesian reconstruction of the data matrix was performed using MrBayes 3.2 (Ronquist & Huelsenbeck 2003) with the best-fitting substitution model (GTR+G). Four Markov chain Monte Carlo (MCMC) chains ran for 2,000,000 generations, sampling every 1000 generations. The first 10% of burn-in trees

were discarded. A majority rule consensus tree was created in order to examine the posterior probabilities (BPP) of each clade. Maximum likelihood (ML) analyses were conducted with RaxML v7.2.6 (Stamatakis 2006) on the T-REX web server (Boc *et al.* 2012) using the model GTR+G. Bootstrap support (BS) was assessed with 1000 replicates.

Yessotoxin analysis

Cultures of two strains of *G. whaseongensis* and seven strains of *G. spinifera* were grown in 200 ml Erlenmeyer flasks under standard culture conditions. At stationary phase, ~10^5 cells were concentrated with a Universal 320 R centrifuge at 850 *g* for 10 min at room temperature. Stationary phase was determined via linear regression of log-transformed cell count time series. Algal pellets for quantification of intracellular YTX were transferred to 2 ml microcentrifuge tubes and stored at –20°C until analysed. Measurements were carried out by liquid chromatography (LC 1100, Agilent, Waldbronn Germany) coupled to tandem mass spectrometry (API 4000 QTrap, Sciex, Darmstadt Germany) as detailed in Wang *et al.* (2019). In brief, separation was performed on a reversed phase column with gradient elution from 40% aqueous methanol–acetonitrile mixture to 100% methanol–acetonitrile. Yessotoxins were screened in the negative mode by selected reaction monitoring (SRM).

RESULTS

Morphology

For species not established in culture only the cyst stages are described, whereas both cyst and thecate stages are described from the cultures available. Cyst morphologies are indicated

by the names of the fossil species which they match. In the following, dimensions given for the cyst central body do not include the processes.

SPINIFERITES BELERIUS

The cyst from Baie de Vilaine, France, from which the hatchling (isolate 18-896, Table 1) was sequenced, was oval, with a central body 37.5 µm long and 32.5 µm wide, with a characteristic, small apical boss (Fig. 1). The archeopyle was not reduced, and was formed by the loss of plate 3″ (Figs 2, 5). The operculum was monoplacate and free. The paracingulum descended with a displacement of twice its width (Fig. 3). The parasulcus was weakly expressed. The cyst had a thin and finely granular wall ornamented with exclusively gonal, trifurcate processes 5.8–13.3 µm long (Figs 3–5). There was one petaloid antapical trumpet-shaped process (Fig. 6).

SPINIFERITES BENTORII

The cyst from Pantan, Croatia, that originated the culture (strain Pantan, Table 1) was pear-shaped, with a central body 53.3 µm long and 43.8 µm wide, with a pronounced apical protuberance (Fig. 7). The paracingulum descended with a displacement of three times its width with no overhang (Fig. 8). The parasulcus was weakly expressed. Processes were exclusively gonal with trifurcate distal ends 9.6–11.7 µm long, with fenestrate bases (Fig. 9). The wall surface was finely granulated. The archeopyle was reduced, formed by the loss of plate 3″ (Fig. 9). The operculum was monoplacate and free. There were two pronounced antapical processes *c.* 14.6 µm in length (Fig. 9). The cyst from Bohai Sea, China (isolate HSN114; Table 1) was pear-shaped, with a central body 62.7 µm long and 64.2 µm wide,

with a pronounced apical protuberance (Fig. S2). Processes were exclusively gonal with trifurcate distal ends 9.0–10.5 µm long. The cells of strain Pantan were 36.7–67.5 µm (46.8 ± 6.9 µm, n = 25) long and 33.3–51.7 µm (41.6 ± 4.7 µm, n = 25) wide with two stout antapical spines 2.3–10.7 µm (6.8 ± 2.5 µm, n = 25) long (Fig. 10). The nucleus was elongated and located in the hyposome. The cingulum was located in the middle of the cell and descended about three times its width with an overhang of four times of its width (Fig. 11). These cells displayed a plate formula of 2pr, 4′, 6″, 6C, 6S, 5‴, 1p, 1⁗. The thecae had a sexiform gonyaulacoid tabulation (Fensome *et al*. 1993, text-fig. 64B) with an S-type ventral organization (Fensome *et al*. 1993, text-figs 82B, D) and neutral torsion (Fensome *et al*. 1993, text-fig. 83B) (Figs 12, 13, 15). The epitheca was conical with pronounced shoulders whereas the hypotheca was trapezoidal. There were six cingular plates of similar size (Fig. 19). The cell surface was thick and reticulated, with numerous trichocyst pores, often at the junctions of the reticulations. The apical pore complex (APC) comprised a pore plate with a lenticular pore inside, surrounded by raised ridges of neighbouring plates, with a small Q plate neighbouring the APC at the right side (Fig. 18).

The first and fourth apical (1′, 4′) plates were narrow and elongated, whereas plates 2′ and 3′ were large and occupied the dorsal part (Fig. 13). There was a ventral pore at the junction of plates 1′, 4′ and Q (Fig. 14). The angle between the major axis and a line joining the ends of the cingulum was approximately 20°. The precingular plates were similar in size except that plate 6″ was triangular and the smallest (Fig. 13). The postcingular plates were similar in size (Figs 15, 16). The antapical (1⁗) plate was seven-sided and asymmetrical, wider than long, located in the middle of the hypotheca (Fig. 15). The posterior intercalary

(1p) plate was narrow and elongated, contacting the left side of plate Sp (Fig. 15). The sulcus comprised the anterior sulcal plate (Sa), anterior left sulcal plate (Ssa), posterior left sulcal plate (Ssp), anterior right sulcal plate (Sda), posterior right sulcal plate (Sdp) and posterior sulcal plate (Sp) (Figs 16, 17). A schematic drawing of the motile cells is provided in Figs 20–23.

SPINIFERITES CF. *BENTORII*

Cysts from the Bohai Sea (isolates WN20, WN21, WN22, Table 1) were pear-shaped, with a central body 49.8–63.9 µm (54.5 ± 6.4 µm, n = 4) long and 43.5–52.8 µm (47.0 ± 4.1 µm, n = 4) wide, with a pronounced apical protuberance (Fig. 24). The wall surface was finely granular. One or two bifurcate intergonal processes were found between each pair of trifurcate gonal processes (Figs 25, 28). The processes were 4.2–7.3 µm long. Process bases were not fenestrate (Figs 27–29). The paracingulum descended with a displacement of three times its width with no overhang (Fig. 27). The parasulcus was weakly expressed. The archeopyle was reduced, formed by the loss of plate 3″ (Fig. 28). The operculum was monoplacate and free.

SPINIFERITES HYPERACANTHUS

The ovoid cyst from the East China Sea that yielded the strain TIO712 (Table 1) had a central body 41.8 µm long and 37.7 µm wide. The cyst had a smooth to finely granular surface. One bifurcate intergonal process was found between each pair of trifurcate gonal processes (Figs 30, 31). Processes were hollow (Fig. 32), 9.0–11.2 µm long, with bases connected by low ridges about 1.5 µm high. Sometimes fenestrate bases could be observed (Fig. 34). The

paracingulum descended with a displacement of its own width. The parasulcus was somewhat expressed. The archeopyle was reduced and precingular, corresponding to plate 3″ (Figs 31, 33). The operculum was monoplacate and free. Cysts formed spontaneously in culture of strain TIO260, which was established through the germination of a single cyst. They were 34.5–40.5 µm long and 31.5–37.0 µm wide, with processes 5.4–12.0 µm long (Figs 33–35).

Thecate cells of strain TIO712 were 27.5–48.3 µm (36.9 ± 7.8 µm, n = 20) long and 22.4–36.6 µm (28.6 ± 5.3 µm, n = 20) wide. The epitheca was conical and the hypotheca was trapezoidal. The cingulum was situated in the equatorial part of the cell and descended about twice its width with a slight overhang (Fig. 36). The angle between the major axis and a line joining the ends of the cingulum was approximately 15°. There were numerous banded chloroplasts in the periphery of the cell and a curved nucleus in the hyposome (Fig. 37). Cells had a plate formula of 2pr, 4′, 6″, 6C, 6S, 5‴, 1p, 1⁗. The theca had a sexiform gonyaulacoid tabulation (Fensome *et al*. 1993, text-fig. 64B) with an S-type ventral organization (Fensome *et al*. 1993, text-figs 82B, D) and dextral torsion (Fensome *et al*. 1993, text-fig. 83C) (Figs 38, 39). Most cells had a long and a short antapical spine on the left and right of posterior sulcal rim, respectively (Fig. 38). Each cell had a short apical horn and a slightly angled shoulder. The cell surface was thick and reticulated with numerous trichocyst pores, often at the junctions of the reticulations. The apical pore complex (APC) comprised a pore plate with a lenticular pore inside, surrounded by raised ridges of neighbouring plates with a small Q plate abutting the APC at the right side (Fig. 42).

Plates 1′ and 4′ were narrow and elongated, with a row of small pores at the right margin of 1′, whereas plates 2′ and 3′ were large and occupied the dorsal part (Figs 40, 41).

There was a ventral pore at the junction of plates 4′ and Q (Fig. 41). Plates 1″ and 2″ were larger than the other precingular plates, with plate 6″ quadrangular and the smallest (Figs 40, 42). The postcingular plates were similar in size (Fig. 43). Plate 1‴′ was hexagonal and asymmetrical, wider than long, located in the middle of the hypotheca. Plate 1p was narrow and elongated, and contacted the left side of plate Sp (Fig. 43). The sulcus comprised plates Sa, Ssa, Ssp, Sda, Sdp and Sp (Fig. 44). The morphology of the cultured strains (GSJZ01, TIO260) was similar to that of strain TIO712 and is not shown here. The morphology of strain TIO1416 was not studied.

SPINIFERITES LAZUS

The cyst from Baie de Vilaine, France, that originated the hatchling (isolate 18-898, Table 1) that was sequenced was oval, with a central body 43.3 µm long and 39.2 µm wide (Fig. 45). The cyst wall was thick with a microgranular surface. Processes were exclusively gonal, 13.3–15.0 µm long, with wide fenestrate bases and connected by low sutural crests. The archeopyle was reduced, formed by the loss of plate 3″ (Fig. 46). The operculum was monoplacate and free. The paracingulum descended with a displacement of three times its width and there was no overhang (Fig. 47). The parasulcus was weakly expressed.

SPINIFERITES MIRABILIS

The cyst from the Gulf of California from which the hatchling (isolate 20-188, Table 1) was sequenced was oval, with a central body 35.4 µm long and 30.4 µm wide (Fig. 48). The cyst wall was microgranular. Gonal processes were 6.7–8.3 µm long, slender and connected by low crests. One or two intergonal processes were present between two adjacent gonal

processes (Fig. 49). A prominent antapical flange connected the two antapical processes, and was approximately 12.1 µm in length (Fig. 48). The paracingulum descended with a displacement of twice its width and there was no overhang (Fig. 49). The parasulcus was weakly expressed. The archeopyle was reduced, formed by the loss of plate 3″ (Fig. 50).

SPINIFERITES RAMOSUS SENSU ROCHON *ET AL.* (1999)

Cysts from the Canadian Pacific giving rise to strains TIO700–TIO705, TIO904, TIO905 (Table 1) were ovoid to spheroidal, with a central body 28.1–46.1 µm (34.9 ± 6.2 µm, n = 8) long and 23.4–36.1 µm (29.3 ± 4.6 µm, n = 8) wide with processes 8.6–13.5 µm long (Fig. 51). Typical gonal processes were 2.8–10.0 µm long and trifurcate with bifurcate tips. The paracingulum descended with a displacement of its own width, without overhang. The parasulcus was weakly expressed. Cysts formed in culture of strain TIO1400 (Table 1) were 27.5–37.5 µm long and 25.0–33.9 µm wide (Figs 52–56). The cyst surface was coarsely granular (Figs 53–55). Occasionally intergonal processes were observed (Fig. 55). The archeopyle was reduced, corresponding to plate 3″ (Fig. 56).

Cells of strain TIO701 had a pronounced apical horn and slightly angled shoulders. The epitheca was conical and the hypotheca was trapezoidal (Fig. 57). The cingulum was located in the equatorial part of the cell and descended about twice of its width with an overhang of one to two widths. The angle between the major axis and a line joining the ends of the cingulum was approximately 15°. There were numerous banded chloroplasts in the periphery and a curved nucleus in the cingular region (Fig. 58). Cells of strain TIO904 were 26.9–41.0 µm (34.8 ± 3.8 µm, n = 31) long and 22.3–32.5 µm (28.8 ± 3.4 µm, n = 31) wide. The plate

formula was 2pr, 4′, 6″, 6C, 6S, 5‴, 1p, 1⁗. Cells often had two antapical spines of similar size, but some cells lacked such spines or had numerous smaller spines. The theca had a sexiform gonyaulacoid tabulation (Fensome *et al*. 1993, text-fig. 64B) with an S-type ventral organization (Fensome *et al*. 1993, text-figs 82B, D) and neutral torsion (Fensome *et al*. 1993, text-fig. 83B) (Figs 59, 60). The cell surface was thick and reticulated, with many trichocyst pores. The apical pore complex comprised a pore plate with a lenticular pore inside, surrounded by raised ridges of neighbouring plates, with a small Q plate abutting the APC at its right side (Fig. 63). Plates 1′ and 4′ were narrow and elongated, whereas plates 2′ and 3′ were large and occupied the dorsal part (Figs 59–61). There was a ventral pore at the junction of plates 4′ and Q (Fig. 63). The precingular plates were similar in size except that plate 6″ was much smaller (Figs 59–62). The postcingular plates were similar in size (Figs 62, 64). Plate 1⁗ was hexagonal and symmetrical, located in the middle of the hypotheca. Plate 1p was narrow and elongated, and contacted the left side of plate Sp (Fig. 64). The sulcus comprised plates Sa, Ssa, Ssp, Sda, Sdp and Sp (Fig. 62). The morphology of the cultured strain TIO1400 was similar to that of strain TIO701 and is not shown here. The morphology of other strains (TIO700, TIO702–TIO705, TIO904, TIO905, TIO1218, WYJ) was not studied.

SPINIFERITES SCABRATUS

The cyst from the Mediterranean Sea from which strain TIO706 (Table 1) was established was oval, with a central body 32.6 μm long and 26.8 μm wide (Fig. 65). There was no apical protuberance. The paracingulum was displaced its own width and the archeopyle was not

reduced, formed by the loss of plate 3″ (Fig. 66). The operculum was free. The processes were hollow and wide at their base *c.* 8.3–11.0 µm in length. The processes were exclusively gonal, and trifurcate with bifurcate tips (Figs 65, 66). The wall surface was coarsely granulate (Fig. 67).

Cells of strain TIO706 had a pronounced apical horn and a slightly angled shoulder. The epitheca was conical and the hypotheca was trapezoidal. There were numerous banded chloroplasts in the periphery and a curved nucleus in the hyposome (Fig. 68). The cingulum was located in the equatorial part of the cell and descended about twice its width with an overhang of two widths (Figs 69, 70). The angle between the major axis and a line joining the ends of the cingulum was approximately 10°. Most cells had two antapical spines of similar size (Fig. 70). Cells were 23.6–35.7 µm (28.1 ± 3.2 µm, n = 19) long and 20.9–33.4 µm (24.6 ± 3.2 µm, n = 19) wide. Cells had the plate formula 1pr, 4′, 6″, 6C, 6S, 5‴, 1p, 1⁗. The theca had a sexiform gonyaulacoid tabulation (Fensome *et al*. 1993, text-fig. 64B) with an S-type ventral organization (Fensome *et al*. 1993, text-figs 82B, D) and neutral torsion (Fensome *et al*. 1993, text-fig. 83B) (Figs 69, 71). The cell surface was thick and reticulated with many trichocyst pores. The apical pore complex comprised a pore plate with a lenticular pore inside, surrounded by raised ridges of neighbouring plates with a small Q plate abutting the APC at the right side (Fig. 72). The sulcus comprised plates Sa, Ssa, Ssp, Sda, Sdp and Sp.

Plates 1′ and 4′ were narrow and elongated without a ventral pore, whereas plates 2′ and 3′ were large and occupied the dorsal part (Figs 69–72). The precingular plates were similar in size except that plate 6″ was much smaller. The postcingular plates were similar in size

(Figs 70, 73). Plate 1′′′′ was hexagonal and symmetrical, located in the middle of the hypotheca. Plate 1p was five-sided and contacted the left side of plate Sp (Fig. 73).

TECTATODINIUM PELLITUM

The cyst from the Gulf of California from which the hatchling (isolate 20-179, table 1) was sequenced was oval, with a central body 49.6 µm long and 43.8 µm wide (Fig. 74). The cyst had an apical protuberance (Fig. 74) and a coarsely granular surface (Fig. 75). The inner wall was thin whereas the outer wall was spongy and 2.9 µm thick, formed by numerous, finely interwoven fibrils (Fig. 76). The archeopyle was large and trapezoidal (Fig. 75).

Molecular phylogeny

All strain and isolate numbers and the corresponding GenBank accession numbers are summarized in Table 1. *Spiniferites hyperacanthus* strains TIO260 and TIO1416 had identical LSU rRNA gene sequences. Sequences of *S. hyperacanthus* strains TIO712 and GSJZ01 were identical to those of *Gonyaulax whaseongensis* A.S. Lim, H.J. Jeong & Ji Hye Kim (GenBank accession: LS481152), but differed from strains TIO260 and TIO1416 in nine positions (99.33% similarity). *Spiniferites ramosus* strains from the Canadian Pacific, the Yellow Sea of China and the East China Sea shared identical sequences but they differed from strain UW323 from the U.K. (Lewis *et al.* 1999; Ellegaard *et al.* 2003; GenBank accession: AY154960) in six positions (99% similarity). Three Chinese isolates of *S.* cf. *bentorii* shared identical sequences but they differed from that of *S. bentorii* from the Adriatic Sea at 14 positions (98.38% similarity). *Spiniferites belerius* from Baie de Vilaine, France differed from Japanese *S. belerius* (GenBank accession: LC222310) at 85 positions (88.09%

similarity) and from *Impagidinium caspienense* (GenBank accession: LC222302) at 20 positions (97.14% similarity).

ML and BI analyses based on LSU rRNA gene sequences yielded similar phylogenetic trees. The BI tree is illustrated in Fig. 77, showing five well-resolved clades, corresponding to families Ceratiaceae, Protoceratiaceae, Pyrophacaceae, Gonyaulacaceae and Lingulodiniaceae. Gonyaulacaceae comprised the fossil genera *Spiniferites, Impagidinium* Stover & Evitt, *Ataxiodinium* P.C. Reid and *Tectatodinium* D. Wall, and the extant genus *Gonyaulax* with maximal support (BPP:1.0, ML BS:100). Species assigned to *Spiniferites* and *Impagidinium* did not form monophyletic groups. The new French *S. belerius* isolate grouped together with *Gonyaulax baltica*/*Impagidinium caspienense* with strong support (BPP:0.95, BS:96), and in turn formed a sister clade to the Japanese *S. belerius* with maximal support. *Spiniferites ramosus* isolates grouped together with maximal support and they formed a sister clade to *S. scabratus* strain TIO706 with maximal support. *Spiniferites hyperacanthus* grouped together with *G. whaseongensis* with maximal support. *Tectatodinium pellitum* formed a clade with *Ataxiodinium choane* with low support. *Spiniferites mirabilis* was a sister clade of *Gonyaulax ellegaardiae* with moderate support (BPP:0.98, BS:79). *Spiniferites bentorii* and *Spiniferites* cf. *bentorii* grouped together with maximal support, and formed a sister clade to *Gonyaulax elongata* with low support.

The SSU rRNA gene sequences of *Spiniferites hyperacanthus* strains TIO260 and TIO712 differed in two positions, and differed from *Gonyaulax whaseongensis* (GenBank accession number: LS481152) in two and four positions respectively (99.80% similarity). *S. bentorii* from the Adriatic Sea differed from isolate HSN114 from Bohai Sea in 112 positions

(93.29% similarity), and differed from *G. spinifera* strain GSTL1 from Malaysia (GenBank accession: AF052190) in 148 positions (91.51% similarity) and from *G. digitalis* in 312 positions (82.07% similarity). ML and BI analyses based on SSU rRNA gene sequences yielded similar phylogenetic trees. The BI tree is illustrated in Fig. 78 showing five well-resolved clades as LSU rRNA gene sequence-based tree. *Spiniferites bentorii* grouped together with Malaysian strain GSTL1 with maximal support, and *Gonyaulax digitalis* formed a clade with several strains of *Gonyaulax ellegaardiae* from the Mediterranean Sea with maximal support.

Yessotoxins

Two strains of *G. whaseongensis* and seven strains of *G. spinifera* were studied for YTXs. None of the YTXs were detected in these strains. The detection limits ranged from 0.1 fg cell^{-1} (*G. spinifera*, TIO904) to 11 fg cell^{-1} (*G. spinifera*, TIO705) depending on the available biomass (Table 2).

DISCUSSION

Morphology

SPINIFERITES BELERIUS AND *S. BENTORII*

Spiniferites belerius is characterized by a relatively small size (35–42 μm long and 28–37 μm wide), bearing a small apical boss and one high antapical, trumpet-shaped process; it is considered to have a wide distribution ranging from tropical to subpolar regions (e.g. Reid 1974; Gurdebeke *et al.* 2018; Limoges *et al.* 2018). Prior to our study, *S. belerius* had been

reported from Japanese waters (Kojima 1989) but only one sequence from a Japanese *S. belerius* was reported (Mertens *et al.* 2018a). It is surprising that our new sequence of *S. belerius* from coastal waters of France differs markedly from the Japanese sequence, although no appreciable morphological separation was observed between them. This suggests that they might belong to a species complex. *Spiniferites belerius* has been related to *Gonyaulax scrippsae* Kofoid (Wall & Dale 1968; Reid 1974). *Gonyaulax scrippsae*, which was described from the San Diego region, California, USA (Kofoid 1911), needs to be restudied from the type locality to establish its resting stage.

Spiniferites bentorii has a pronounced apical boss, a pear shape and generally two more developed antapical processes (e.g. Rossignol 1964; Limoges *et al.* 2018). Intergonal processes are only occasionally present in *S. bentorii*, but in our specimens from Bohai Sea, China, they are constantly present, and for that reason these specimens were identified as *Spiniferites* cf. *bentorii*. *Gonyaulax digitalis* is an obscure species described by Pouchet (1883) from Concarneau Bay, France. No size was given by Pouchet, but a significant displacement of the cingulum and two antapical spines can be observed in his illustrations. *Gonyaulax digitalis* has been connected previously to *Spiniferites bentorii* (Wall & Dale 1968, 1970). However, the SSU rRNA gene sequences of *G. digitalis* from the type locality (Concarneau Bay) is reported here for the first time and is phylogenetically separated from the strain originated from cysts with the morphology of *S. bentorii* (Fig. 78); we describe this strain as a new species, *Gonyaulax nezaniae sp. nov*. Another cyst-defined species, *Bitectatodinium tepikiense* has also been related with *Gonyaulax digitalis* (Lewis *et al.* 2001), but the cyst has not been found in Concarneau (K.N. Mertens, personal observations) and the

two species appear distantly related (Figs 77, 78). This suggests that modern cysts with *B. tepikiense* morphology may correspond to an undescribed species of *Gonyaulax*, perhaps related to the specimen of *G. digitalis* described by Kofoid (1911) from the Faeroe Islands. Differences between *G. nezaniae*, *G. digitalis sensu stricto* and the motile stage derived from *B. tepikiense*-like cysts are summarized in Table 3. *Gonyaulax digitalis sensu stricto* is not sufficiently known and needs further study.

SPINIFERITES HYPERACANTHUS AND *S. MIRABILIS*

Spiniferites hyperacanthus and *S. mirabilis* are morphologically similar. Both of them are spherical, with a variable number of intergonal processes, but differ in the absence of a well-developed flange along the suture between the antapical plate and plate 3‴ in *S. hyperacanthus* (Fig. 30), which is present in *S. mirabilis* (Fig. 48). Although both species have sometimes been grouped in palynological counts (e.g. Limoges *et al.* 2013), our study demonstrates that they are clearly distinct species. *Spiniferites hyperacanthus* was originally described from the Middle Miocene of Balcombe Bay by Deflandre & Cookson (1955). Their holotype is significantly larger than our specimen, having a central body diameter of 54–59 μm and processes 13–20 μm long. However, other specimen identified as *S. hyperacanthus* from Japan by Matsuoka (1985) have similar sizes to our specimen (38.2–40.3 μm long and 34–38.5 μm wide; process length 12.0–18.5 μm). *Spiniferites hyperacanthus* from Tokyo Bay has been connected to the *Gonyaulax spinifera* complex (Matsuoka *et al.* 2003), but here we demonstrate that the motile stages correspond to *Gonyaulax whaseongensis*, which is characterized by two unequal antapical spines, a quadrangular plate 6″ and a ventral pore at

the junction of plates 4′ and Q (Lim *et al.* 2018). In addition, our cells show a dextral torsion, also reported in *G. whaseongensis* (Lim *et al.* 2018), whereas in *G. digitalis* and *G. spinifera* there is a neutral torsion (Kofoid 1911). *Spiniferites hyperacanthus* from Chinese coastal waters and *G. whaseongensis* also have identical molecular sequences, further indicating that they are conspecific. Our strain TIO260 produces cysts in culture spontaneously, but the Korean strain did not generate cysts in culture (Lim *et al.* 2018), suggesting that this species might be heterothallic. Our strain was established from an assumed sexual resting cyst that produced daughter cells through meiosis (Elbrächter 2003) whereas the Korean strain is from a single, presumably vegetative cell (Lim *et al.* 2018). Our specimen of *S. mirabilis* has one or two intergonal processes along each major suture, and may therefore be identified as *S. mirabilis* subsp. *mirabilis* (Rossignol 1964). *Spiniferites mirabilis* has been connected to *Gonyaulax spinifera*, which has a variable number of small antapical spines, with two of them prominent (Wall & Dale 1968; Morquecho *et al.* 2009).

SPINIFERITES LAZUS AND *SPINIFERITES SCABRATUS*

Spiniferites lazus is characterized by having exclusively gonal processes with wide fenestrate bases (Reid 1974), and our specimen fits the original description well. The cyst of *Spiniferites scabratus* from Corsica matches the original description of *S. scabratus* in terms of microgranular septa with exclusively gonal and hollow processes, and an archeopyle that is not reduced (Mertens *et al.* 2018b). The motile cells of strain TIO706 are morphologically similar to *Gonyaulax spinifera* but they are smaller and lack a ventral pore. A resting cyst

identified as *S. scabratus* from the Gulf of Paria yielded a motile cell without antapical spines and with very indistinct ornamentation (Wall & Dale 1968).

SPINIFERITES RAMOSUS SENSU ROCHON ET AL. (1999)

The taxonomic history of *S. ramosus* is complicated and we refer to Mertens *et al.* (2018b, p. 34) for more information. For modern cysts, the informal taxon *S. ramosus sensu* Rochon *et al*. (1999) is characterized by possessing exclusively gonal processes and a smooth wall. Our studied specimens had a granular wall, but were nearly identical molecularly (99% similarity) with smooth-walled *S. ramosus* cysts documented by Ellegaard *et al*. (2003), who connected this species to *Gonyaulax* cf. *spinifera*. Our cysts are similar to *Spiniferites ramosus* from the North Sea, which shows a weakly granulate surface, occasional intergonal process and a reduced archeopyle (Lewis *et al.* 1999). Our motile cells are also morphologically similar to those of Lewis *et al.* (1999) in having a pronounced apical horn, a girdle displacement of two cingulum widths, a ventral pore at the junction of plates 4′ and Q, and two antapical spines.

TECTATODINIUM PELLITUM

Living cysts with the morphology of *T. pellitum* have been reported in sediments of Massachusetts, USA, and of the Gulf of California, Mexico; the germinated cells had two antapical spines and were connected to *Gonyaulax spinifera* (Wall & Dale 1967, 1968; Morquecho *et al.* 2009). The identity of the motile stage, however, remains to be determined as its molecular sequence is quite different from that of *G. spinifera*. *Tectatodinium pellitum* is a coastal subtropical to equatorial species (Zonneveld *et al.* 2013) but it can be occasionally found in estuarine temperate waters (e.g. Pospelova *et al.* 2004).

Molecular phylogeny

Our results suggest that species of the fossil genera *Spiniferites* and *Impagidinium*, as currently circumscribed, are polyphyletic (Mertens *et al.* 2018a) because species of *Bitectatodinium*, *Ataxiodinium* and *Tectatodinium* group with those of *Spiniferites* and *Impagidinium*. The phylogenetic positions of *S. bentorii*, *S. mirabilis*, *S. lazus*, *S. scabratus* and *S. hyperacanthus* are inferred here for the first time. Each of these species forms a distinct clade, supporting the idea that there is a large diversity within *Spiniferites*. The extant genus *Gonyaulax* appears to be related to several fossil genera, and the tabulation of *Gonyaulax* fits well with the paratabulation of *Spiniferites* and *Impagidinium*, suggesting that it has changed very little during evolution. In contrast, species of *Bitectatodinium*, *Ataxiodinium* and *Tectatodinium* do not display a paratabulation (Reid 1974). These genera do not group together in the molecular phylogeny, suggesting that paratabulation has been lost several times during evolution.

It has been suggested to unite the biological and paleobiological nomenclatures by retaining *Gonyaulax* as a very large genus and subdividing it (e.g. subgenera) using fossil names such as *Spiniferites*, *Impagidinium*, and *Bitectatodinium* (Ellegaard *et al.* 2018). However, with their current circumscription, the subgenera remain polyphyletic. The presence or absence of an apical boss and intergonal processes are useful to differentiate *Spiniferites* species. However, *S. belerius* and *S. bentorii* do not group together although they share an apical boss. On the other hand, *S. bentorii* with and without intergonal processes group together suggesting that presence or absence of intergonal processes alone is not

enough to differentiate species. An integrated analysis of multiple morphological features might be necessary to classify this group of dinoflagellate species.

The genus *Gonyaulax* was initially proposed to be subdivided into four subgenera, i.e. *Gonyaulax* subg. *Gonyaulax*, *G.* subg. *Fusigonyaulax* Kofoid, *G.* subg. *Steiniella* (F. Schütt) Kofoid and *G.* subg. *Acanthogonyaulax* Kofoid, based upon the general shape of the motile cells (Kofoid 1911). *Gonyaulax* subg. *Gonyaulax* was further subdivided into the *spinifera*, *polygramma* and *sphaeroidea* groups. Unfortunately, neither the subgenera nor the groups appear monophyletic. However, few sequences are presently available for the subgenus *Steiniella*, and so far none is available from subgenera *Fusigonyaulax* and *Acanthogonyaulax*. Plate 4′ comprises two parts, named 4′a and 4′p, in *G. fragilis* (F. Schütt) Kofoid and *G. hyalina* Ostenfeld & E.J. Schmidt (Carbonell-Moore & Mertens 2019), which have been classified within *Gonyaulax* subg. *Steiniella*, but plate 4′ is not divided in other subgenera. Whether molecular phylogenies support the subgenus *Steiniella* remains to be determined.

Although Wall & Dale (1968) linked *Gonyaulax spinifera* and *G. digitalis* to at least five cyst morphotypes, they observed that a naturally occurring population of motile cells produced only one cyst morphotype. It is highly likely that several genetically different species exist with morphologies very similar to *G. spinifera* and *G. digitalis*. *Gonyaulax spinifera* needs to be more narrowly characterized, preferably from the analysis of populations from the type locality (western coast of Norway). With narrowly defined extant species it may become possible to find connections to cysts corresponding in morphology to *S. belerius*, *S. lazus*, *S. mirabilis*, *S. scabratus* and *T. pellitum*, as has been exemplified for *Gonyaulax elongata* (basionym *Spiniferites elongatus*) and *Gonyaulax membranacea*

(previously known as *Spiniferites membranaceus*) (Ellegaard *et al.* 2003). Alternatively, for names based on fossil cysts, a new name may be created, e.g. *Gonyaulax ellegaardiae* was described based on motile cells germinated from *S. pachydermus*-like cysts (Mertens *et al.* 2015). Two analogous situations are suggested by our observations on *G. whaseongensis* and *S. hyperacanthus*-like cysts, and on *G. nezaniae* and *S. bentorii*-like cysts.

Yessotoxin

Some strains designated as *Gonyaulax spinifera* are known as producers of yessotoxins. For example, a strain of *G. spinifera* from New Zealand produces YTXs at levels approximately 20-fold higher than *Protoceratium reticulatum* (Claparède & J. Lachmann) Buetschli (Rhodes *et al.* 2006), but molecular phylogeny suggests that this strain in fact is closer to *Gonyaulax ellegaardiae* (Mertens *et al.* 2015), which might explain why we failed to detect yessotoxins in our strains of *G. spinifera*. Similar remarks can be made concerning a *G. spinifera* strain reported by Pitcher *et al.* (2019). Even though the authors described the species as *G. spinifera* based on morphological characteristics, the phylogeny clearly locates the species in the *G. membranacea* clade (Pitcher *et al.* 2019), which leads to conclusion that these two reports of YTX-producing *G. spinifera* are based on misidentifications. The lack of YTX-production of *G. spinifera* found in this study is consistent with other reports of non-toxigenic *G. spinifera* in the North (Krock *et al.* 2006) and South Atlantic (Krock *et al.* 2015). This raises the question of whether *G. spinifera sensu stricto* is erroneously considered an YTX-producer or if this species comprises toxigenic and non-toxigenic genotypes.

Formal taxonomic description

Gonyaulax nezaniae* H. Gu & K.N. Mertens *sp. nov.

Figs 10–23

DESCRIPTION: Cells were 37–68 µm long and 33–52 µm wide with two stout antapical spines 2–11 µm long. The epitheca was conical with pronounced shoulders. The cell surface was thick and reticulated. The cingulum was located in the equatorial part of the cell and descended about three times its width. Cells displayed a plate formula of 2pr, 4′, 6″, 6C, 6S, 5‴, 1p, 1⁗. There was a ventral pore at the junction of plates 1′, 4′ and Q. The angle between the major axis and a line joining the ends of the cingulum was approximately 20°. The cyst was pear-shaped, 53–63 µm long and 44–64 µm wide with a pronounced apical protuberance. The paracingulum descended with a displacement of three times its width. Processes were exclusively gonal, 10–12 µm long, and had fenestrate bases. The archeopyle was reduced and corresponded to the third precingular plate.

HOLOTYPE: SEM stub of thecate cells from a culture established from a cyst extracted from sediment of Pantan, Croatia, stored at the CEDiT (Centre of Excellence for Dinophyte Taxonomy) dinoflagellate type collection, Wilhelmshaven, Germany with the code CEDiT2021H123.

TYPE LOCALITY: Pantan, Croatia (Adriatic Sea; 43°31.26'N, 16°16.38'E). Collection date: 4 May 2017.

HABITAT: Marine and planktonic.

ETYMOLOGY: The epithet '*nezaniae*' is in honour of Dr. Elisabeth Nézan for her significant contributions to dinoflagellate taxonomy.

GENBANK ACCESSION: MW793450 and MW775690, respectively nuclear-encoded SSU and LSU rRNA gene sequence.

CONCLUSION

Seven out of 13 known extant cysts with morphologies matching *Spiniferites* species were examined in the present study. The motile stage of cysts morphologically resembling *S. bentorii* was assigned to a new species, *Gonyaulax nezaniae*. Although the cyst-theca relationships of *Spiniferites scabratus* was established, the identity of motile stages remains to be determined. The current cyst-theca relationships inferred for *Spiniferites* and related species is summarized in Table 4, but those of *S. belerius*, *S. mirabilis*, *S. lazus*, *Spiniferites* cf. *bentorii* and *Tectatodinium pellitum* have not yet been resolved. A detailed investigation of *Gonyaulax spinifera* and *G. digitalis* from their type localities is essential to fully understand the stages of the life cycle of *Spiniferites* and related genera. Future efforts to investigate the relation of these fossil species to *Gonyaulax* are urgently needed.

ACKNOWLEDGEMENTS

The Regional Council of Brittany, the General Council of Finistère and the urban community of Concarneau-Cornouaille-Agglomération are acknowledged for the funding of the Sigma 300 FE-SEM of the station of Marine Biology in Concarneau. Elisabeth Nézan is thanked for isolating *Gonyaulax digitalis* from Concarneau.

FUNDING

This work was supported by the National Natural Science Foundation of China (42076085, 42030404), the National Key Research and Development Program of China (2019YFE0124700). Funding for collection of sediments in coastal waters of British

Columbia (Canada) was provided by a Natural Sciences and Engineering Research Council of Canada (NSERC) Discovery grant to VP. Sediment collection at Isla San José, Gulf of California was supported by CIBNOR projects PC013 and 20014. Collecting the sediments in the Croatian coastal water was funded by the Croatian Science Foundation under the project (IP-2014-09-3606), MARIPLAN.

REFERENCES

Álvarez G., Uribe E., Regueiro J., Blanco J. & Fraga S. 2016. *Gonyaulax taylorii*, a new yessotoxins-producer dinoflagellate species from Chilean waters. *Harmful Algae* 58: 8–15.

Balech E. 1980. On the thecal morphology of dinoflagellates with special emphasis on circular and sulcal plates. *Anales del Centro de Ciencias del Mar y Limnologia, Universidad Nacional Autonomia de Mexico* 7: 57–68.

Boc A., Diallo A.B. & Makarenkov V. 2012. T-REX: a web server for inferring, validating and visualizing phylogenetic trees and networks. *Nucleic Acids Research* 40: W573–W579.

Carbonell-Moore M.C. & Mertens K.N. 2019. Should *Gonyaulax hyalina* and *Gonyaulax fragilis* (Dinophyceae) remain two different taxa? *Phycologia* 58: 685–689.

Chikwililwa C., McCarron P., Waniek J.J. & Schulz-Bull D.E. 2019. Phylogenetic analysis and yessotoxin profiles of *Gonyaulax spinifera* cultures from the Benguela Current upwelling system. *Harmful Algae* 85: Article 101626.

Chomérat N. & Couté A. 2008. *Protoperidinium bolmonense* sp. nov. (Peridiniales, Dinophyceae), a small dinoflagellate from a brackish hypereutrophic lagoon (South of France). *Phycologia* 47: 392–403.

Ciminiello P., Fattorusso E., Forino M., Magno S., Poletti R. & Viviani R. 1998. Isolation of adriatoxin, a new analogue of yessotoxin from mussels of the Adriatic Sea. *Tetrahedron Letter* 39: 8897–8900.

Dale B. 1976. Cyst formation, sedimentation, and preservation: factors affecting dinoflagellate assemblages in recent sediments from Trondheimsfjord, Norway. *Review of Palaeobotany and Palynology* 22: 39–60.

Deflandre G. & Cookson I.C. 1955. Fossil microplankton from Australian late Mesozoic and Tertiary sediments. *Marine and Freshwater Research* 6: 242–314.

Diesing K.M. 1866. Revision der Prothelminthen. Abtheilung: Mastigophoren. *Sitzungsberichte der Kaiserlichen Akademie der Wissenschaften, Mathematisch-Naturwissenschaftliche Classe* 52: 287–401.

Dodge J. 1989. Some revisions of the family Gonyaulacaceae (Dinophyceae) based on a scanning electron microscope study. *Botanica Marina* 32: 275–298.

Domínguez H.J., Souto M.L., Norte M., Daranas A.H. & Fernández J.J. 2010. Adriatoxin-B, the first C-13 terminal truncated YTX analogue obtained from dinoflagellates. *Toxicon* 55: 1484–1490.

Elbrächter M. 2003. Dinophyte reproduction: progress and conflicts. *Journal of Phycology* 39: 629–632.

Ellegaard M., Lewis J. & Harding I.C. 2002. Cyst-theca relationship, life cycle, and effects of temperature and salinity on the cyst morphology of *Gonyaulax baltica* sp. nov. (Dinophyceae) from the Baltic Sea area. *Journal of Phycology* 38: 775–789.

Ellegaard M., Daugbjerg N., Rochon A., Lewis J. & Harding I. 2003. Morphological and LSU rDNA sequence variation within the *Gonyaulax spinifera*-Spiniferites group (Dinophyceae) and proposal of *G. elongata* comb. nov. and *G. membranacea* comb. nov. *Phycologia* 42: 151–164.

Ellegaard M., Head M.J. & Versteegh G.J. 2018. Linking biological and geological data on dinoflagellates using the genus *Spiniferites* as an example: the implications of species concepts, taxonomy and dual nomenclature. *Palynology* 42: 221–230.

Fensome R.A., Taylor F.J.R., Norris G., Sarjeant W.A.S., Wharton D.I. & Williams G.L. 1993. A classification of fossil and living dinoflagellates. *Micropaleontology Special Publication* 7: 1–351.

Guillard R.R.L. & Ryther J.H. 1962. Studies of marine planktonic diatoms. I. *Cyclotella nana* Hustedt and *Detonula confervacea* Cleve. *Canadian Journal of Microbiology* 8: 229–239.

Gurdebeke P.R., Mertens K.N., Bogus K., Marret F., Chomérat N., Vrielinck H. & Louwye S. 2018. Taxonomic re-investigation and geochemical characterization of Reid's (1974) species of *Spiniferites* from holotype and topotype material. *Palynology* 42: 93–110.

Hall T.A. 1999. BioEdit: a user-friendly biological sequence alignment editor and analysis program for Windows 95/98/NT. *Nucleic Acids Symposium Series* 41: 95–98.

Head M.J., Fensome R.A., Herendeen P.S. & Skog J.E. 2016. (315–319) Proposals to amend Article 11.8 and its Examples to remove ambiguity in the sanctioning of dual nomenclature for dinoflagellates, and an emendation of Article 11.7, Example 29. *Taxon* 65: 902–903.

Katoh K. & Standley D.M. 2013. MAFFT multiple sequence alignment software version 7: improvements in performance and usability. *Molecular Biology and Evolution* 30: 772–780.

Kofoid C.A. 1909. On *Peridinium steini* Jörgensen, with a note on the nomenclature of the skeleton of the Peridinidae. *Archiv für Protistenkunde* 16: 25–47.

Kofoid C.A. 1911. Dinoflagellata of the San Diego region, IV. The genus *Gonyaulax* with notes on its skeletal morphology and a discussion of its generic and specific characters. *University of California Publication in Zoology* 8: 187–286.

Kojima N. 1989. Dinoflagellate cyst analysis of Holocene sediments from Lake Hamana in central Japan. *Transactions and Proceedings of the Paleontological Society of Japan, New series* 155: 197–211.

Krock B., Alpermann T.J., Tillmann U., Pitcher G.C. & Cembella A.D. 2006. Yessotoxin profiles of the marine dinoflagellates *Protoceratium reticulatum* and *Gonyaulax spinifera*. 12th International Conference on Harmful Algae, Copenhagen, Denmark, ISSHA & IOC of UNESCO.

Krock B., Borel C.M., Barrera F., Tillmann U., Fabro E., Almandoz G.O., Ferrario M., Cardona J.E.G., Koch B.P. & Alonso C. 2015. Analysis of the hydrographic conditions and cyst beds in the San Jorge Gulf, Argentina, that favor dinoflagellate population development including toxigenic species and their toxins. *Journal of Marine Systems* 148: 86–100.

Lewis J., Rochon A. & Harding I. 1999. Preliminary observations of cyst-theca relationships in *Spiniferites ramosus* and *Spiniferites membranaceus* (Dinophyceae). *Grana* 38: 113–124.

Lewis J., Rochon A., Ellegaard M., Mudie P.J. & Harding I.C. 2001. The cyst-theca relationship of *Bitectatodinium tepikiense* (Dinophyceae). *European Journal of Phycology* 36: 137–146.

Lim A.S., Jeong H.J., Kwon J.E., Lee S.Y. & Kim J.H. 2018. *Gonyaulax whaseongensis* sp. nov. (Gonyaulacales, Dinophyceae), a new phototrophic species from Korean coastal waters. *Journal of Phycology* 54: 923–928.

Limoges A., Londeix L. & de Vernal A. 2013. Organic-walled dinoflagellate cyst distribution in the Gulf of Mexico. *Marine Micropaleontology* 102: 51–68.

Limoges A., Londeix L., Mertens K.N., Rochon A., Pospelova V., Cuéllar T. & de Vernal A. 2018. Identification key for Pliocene and Quaternary *Spiniferites* taxa bearing intergonal

processes based on observations from estuarine and coastal environments. *Palynology* 42: 72–88.

Luo Z., Mertens K.N., Nézan E., Gu L., Pospelova V., Thoha H. & Gu H. 2019. Morphology, ultrastructure and molecular phylogeny of cyst-producing *Caladoa arcachonensis* gen. et sp. nov. (Peridiniales, Dinophyceae) from France and Indonesia. *European Journal of Phycology* 54: 235–248.

Matsuoka K. 1985. Organic-walled dinoflagellate cysts from surface sediments of Nagasaki Bay and Senzaki Bay, West Japan. *Faculty of Liberal Arts, Nagasaki University, Natural Science* 25: 21–115.

Matsuoka K., Joyce L.B., Kotani Y. & Matsuyama Y. 2003. Modern dinoflagellate cysts in hypertrophic coastal waters of Tokyo Bay, Japan. *Journal of Plankton Research* 25: 1461–1470.

Medlin L., Elwood H.J., Stickel S. & Sogin M.L. 1988. The characterization of enzymatically amplified eukaryotic 16S-like rRNA-coding regions. *Gene* 71: 491–499.

Mertens K.N. & Carbonell-Moore C. 2018. Introduction to *Spiniferites* Mantell 1850 special issue. *Palynology* 42: 1–9.

Mertens K.N., Aydin H., Uzar S., Takano Y., Yamaguchi A. & Matsuoka K. 2015. Relationship between the dinoflagellate cyst *Spiniferites pachydermus* and *Gonyaulax ellegaardiae* sp. nov. from Izmir Bay, Turkey, and molecular characterization. *Journal of Phycology* 51: 560–573.

Mertens K.N., Takano Y., Gu H., Bagheri S., Pospelova V., Pieńkowski A.J., Leroy S. & Matsuoka K. 2018a. Cyst-theca relationship and phylogenetic position of *Impagidinium caspienense* incubated from Caspian Sea surface sediments: Relation to *Gonyaulax baltica* and evidence for heterospory within Gonyaulacoid dinoflagellates. *Journal of Eukaryotic Microbiology* 64: 829–842.

Mertens K.N., Van Nieuwenhove N., Gurdebeke P.R., Aydin H., Bogus K., Bringué M., Dale B., De Schepper S., de Vernal A., Ellegaard M. *et al.* 2018b. The dinoflagellate cyst genera *Achomosphaera* Evitt 1963 and *Spiniferites* Mantell 1850 in Pliocene to modern sediments: a summary of round table discussions. *Palynology* 42: 10–44.

Miles C.O., Samdal I.A., Aasen J.A., Jensen D.J., Quilliam M.A., Petersen D., Briggs L.M., Wilkins A.L., Rise F. & Cooney J.M. 2005. Evidence for numerous analogs of yessotoxin in *Protoceratium reticulatum*. *Harmful Algae* 4: 1075–1091.

Morquecho L., Góngora-González D.T. & Okolodkov Y.B. 2009. Cyst-theca relationships of Gonyaulacales and Peridiniales (Dinophyceae) from Bahía Concepción, Gulf of California. *Acta Botanica Mexicana* 88: 9–29.

Murata M., Kumagai M., Lee J.S. & Yasumoto T. 1987. Isolation and structure of yessotoxin, a novel polyether compound implicated in diarrhetic shellfish poisoning. *Tetrahedron Letters* 28: 5869–5872.

Pitcher G.C., Foord C.J., Macey B.M., Mansfield L., Mouton A., Smith M.E., Osmond S.J. & Van Der Molen L. 2019. Devastating farmed abalone mortalities attributed to yessotoxin-producing dinoflagellates. *Harmful Algae* 81: 30–41.

Posada D. 2008. jModelTest: phylogenetic model averaging. *Molecular Biology and Evolution* 25: 1253–1256.

Pospelova V., Chmura G.L. & Walker, H.A. 2004. Environmental factors influencing spatial distribution of dinoflagellate cyst assemblages in shallow lagoons of southern New England (USA). *Review of Palaeobotany and Palynology* 128: 7–34.

Pouchet G. 1883. Contribution à l'histoire des cilio-flagellés. *Journal de l'Anatomie et de la Physiologie Normales et Pathologiques de l'Homme et des Animaux* 19: 399–455.

Price A.M. & Pospelova V. 2014. *Spiniferites multisphaerus*, a new dinoflagellate cyst from the Late Quaternary of the Guaymas Basin, Gulf of California, Mexico. *Palynology* 38: 101–116.

Reid P. 1974. Gonyaulacacean dinoflagellate cysts from the British Isles. *Nova Hedwigia* 25: 579–637

Rhodes L., McNabb P., De Salas M., Briggs L., Beuzenberg V. & Gladstone M. 2006. Yessotoxin production by *Gonyaulax spinifera*. *Harmful Algae* 5: 148–155.

Riccardi M., Guerrini F., Roncarati F., Milandri A., Cangini M., Pigozzi S., Riccardi E., Ceredi A., Ciminiello P. & Dell'Aversano C. 2009. *Gonyaulax spinifera* from the Adriatic sea: Toxin production and phylogenetic analysis. *Harmful Algae* 8: 279–290.

Rochon A., Vernal A.D., Turon J.L., Matthiessen J. & Head M.J. 1999. Distribution of recent dinoflagellate cysts in surface sediments from the North Atlantic Ocean and adjacent seas in relation to sea-surface parameters. *American Association of Stratigraphic Palynologists Contribution Series* 35: 1–146.

Rochon A., Lewis J., Ellegaard M. & Harding I.C. 2009. The *Gonyaulax spinifera* (Dinophyceae) "complex": Perpetuating the paradox? *Review of Palaeobotany and Palynology* 155: 52–60.

Ronquist F. & Huelsenbeck J.P. 2003. MrBayes 3: Bayesian phylogenetic inference under mixed models. *Bioinformatics* 19: 1572–1574.

Rossignol M. 1964. Hystrichosphères du Quaternaire en Méditerranée orientale, dans les sédiments Pléistocènes et les boues marines actuelles. *Revue de Micropaléontologie* 7: 83–99.

Sarjeant W. 1970. The genus *Spiniferites* Mantell, 1850 (Dinophyceae). *Grana* 10: 74–78.

Stamatakis A. 2006. RAxML-VI-HPC: maximum likelihood-based phylogenetic analyses with thousands of taxa and mixed models. *Bioinformatics* 22: 2688–2690.

Turland N.J., Wiersema J.H., Barrie F.R., Greuter W., Hawksworth D.L., Herendeen P.S., Knapp S., Kusber W.-H., Li D.-Z., Marhold K. *et al.* [Eds] 2018. *International Code of Nomenclature for algae, fungi, and plants (Shenzhen Code) adopted by the Nineteenth International Botanical Congress Shenzhen, China, July 2017*. Koeltz Botanical Books, Glashütten, Germany. xxxviii + 254 pp. [*Regnum Vegetabile* 159] DOI https://doi.org/10.12705/Code.2018

Wall D. 1965. Modern hystrichospheres and dinoflagellate cysts from the Woods Hole region. *Grana* 6: 297–314.

Wall D. & Dale B. 1966. "Living Fossils" in Western Atlantic Plankton. *Nature* 211: 1025–1026.

Wall D. & Dale B. 1967. The resting cysts of modern marine dinoflagellates and their palaeontological significance. *Review of Palaeobotany and Palynology* 2: 349–354.

Wall D. & Dale B. 1968. Modern dinoflagellate cysts and evolution of the Peridiniales. *Micropaleontology* 14: 265–304.

Wall D. & Dale B. 1970. Living hystrichosphaerid dinoflagellate spores from Bermuda and Puerto Rico. *Micropaleontology* 16: 47–58.

Wang N., Mertens K.N., Krock B., Luo Z., Derrien A., Pospelova V., Liang Y., Bilien G., Smith K.F., De Schepper S., Wietkamp S., Tillmann U. & Gu H. 2019. Cryptic speciation in *Protoceratium reticulatum* (Dinophyceae): evidence from morphological, molecular and ecophysiological data. *Harmful Algae* 88: Article 101610.

Williams G.L., Fensome R.A. & MacRae R.A. 2017. DINOFLAJ3. American Association of Stratigraphic Palynologists, Data Series no. 2. http://dinoflaj.smu.ca/dinoflaj3.

Zonneveld K.A., Marret F., Versteegh G.J., Bogus K., Bonnet S., Bouimetarhan I., Crouch E., de Vernal A., Elshanawany R., Edwards L. *et al.* 2013. Atlas of modern dinoflagellate cyst

distribution based on 2405 data points. *Review of Palaeobotany and Palynology* 191: 1–197.

FIGURE CAPTIONS

Figs 1–9. Light (LM) and scanning electron micrographs (SEM) of modern cysts with the morphologies of *Spiniferites belerius* from Baie de Vilaine, France, and *Spiniferites bentorii* from Pantan, Croatia. Scale bars = 10 μm.

Fig. 1. *Spiniferites belerius*, LM, mid focus of ventral view of an empty cyst, showing the apical protuberance (arrow).

Fig. 2. *Spiniferites belerius*, LM, high focus of dorsal view of an empty cyst, showing the archeopyle.

Fig. 3. *Spiniferites belerius*, LM, high focus of ventral view of an empty cyst, showing the cingulum (arrows).

Fig. 4. *Spiniferites belerius*, LM, high focus of dorsal view of an empty cyst.

Fig. 5. *Spiniferites belerius*, SEM, dorsal view of cyst, showing the archeopyle.

Fig. 6. *Spiniferites belerius*, SEM, antapical view of cyst, showing the trumpet-like process (arrow).

Fig. 7. *Spiniferites bentorii*, LM, mid focus of ventral view of an empty cyst, showing the apical boss (arrow).

Fig. 8. *Spiniferites bentorii*, LM, high focus of ventral view of an empty cyst, showing the cingulum displacement.

Fig. 9. *Spiniferites bentorii*, SEM, dorsal view of an empty cyst, showing the reduced archeopyle, the fenestrations at the base of processes (arrows) and two antapical processes (arrowheads).

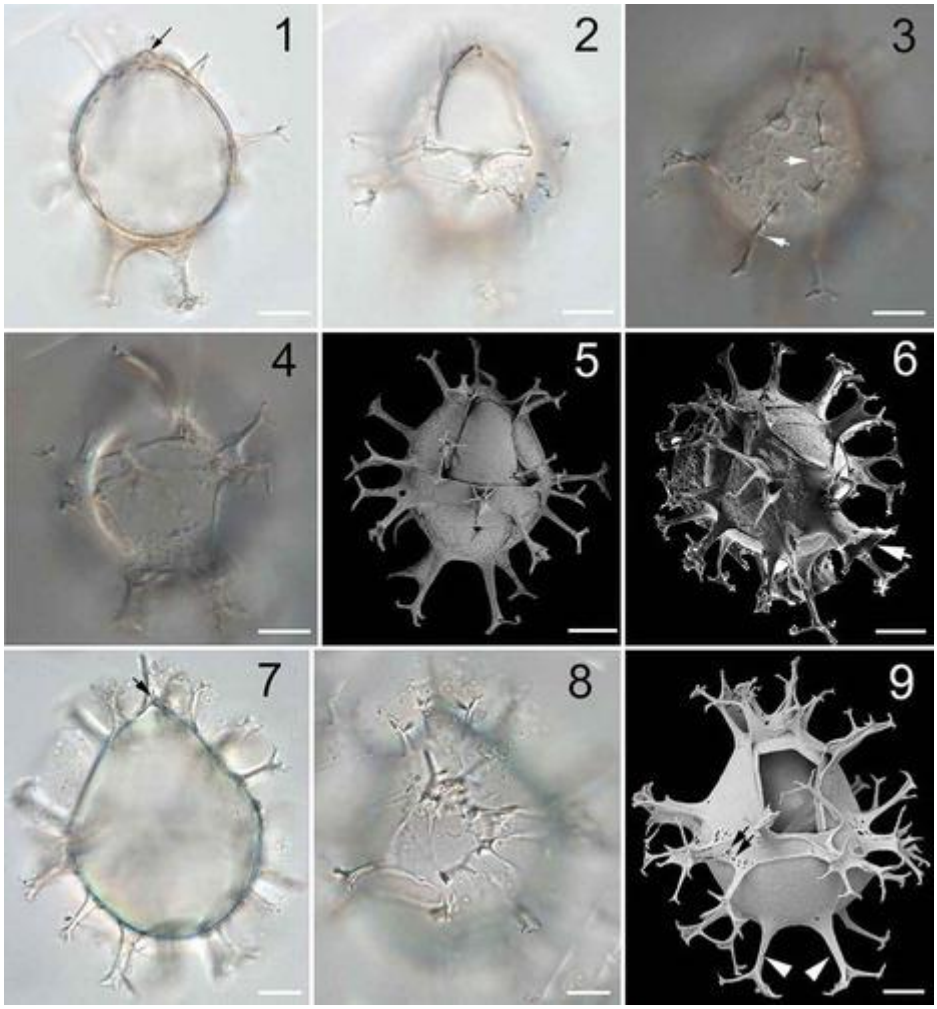

Figs 10–19. Motile cells from culture originated from *Spiniferites bentorii*-like cysts from Croatia, LM and SEM.

Fig. 10. Mid focus of a living cell, showing two stout antapical spines (LM). Scale bar = 10 μm.

Fig. 11. Ventral view of a cell showing cingulum displacement (SEM). Scale bar = 10 μm.

Fig. 12. A cell in dorsal view showing neutral torsion (SEM). Scale bar = 10 μm.

Fig. 13. Apical view of a cell showing four apical plates (1′–4′) and six precingular plates (1″–6″) (SEM). Scale bar = 10 μm.

Fig. 14. Ventral view of a cell showing a ventral pore (arrow) (SEM). Scale bar = 5 μm.

Fig. 15. Antapical view of a cell showing the five postcingular plates (*2‴–*6‴), one antapical plate (1‴′) and one posterior intercalary plate (1p, SEM). Scale bar = 10 μm.

Figs 16, 17. Internal view showing the anterior sulcal plate (Sa), left anterior sulcal plate (Ssa), left posterior sulcal plate (Ssp), anterior right sulcal plate (Sda), posterior right sulcal plate (Sdp) and posterior sulcal plate (Sp, SEM). Scale bars = 5 μm.

Fig. 18. Apical view showing the apical pore complex (apc) and a Q plate (SEM). Scale bar = 2 μm.

Fig. 19. A broken cell showing six cingular plates (SEM). Scale bar = 10 μm.

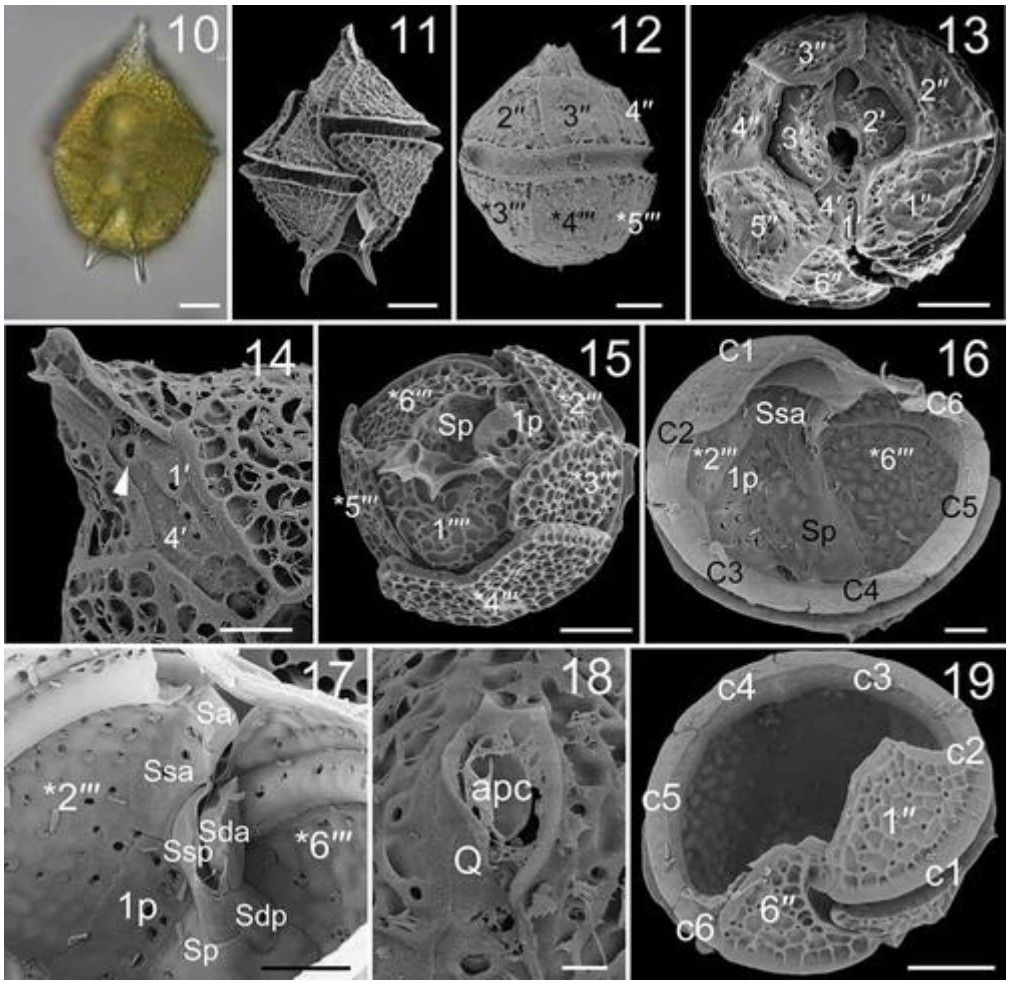

Figs 20–23. Schematic representation of motile cells originated from *Spiniferites bentorii*-like cysts.

Fig. 20. Ventral view.

Fig. 21. Dorsal view.

Fig. 22. Apical view.

Fig. 23. Antapical view.

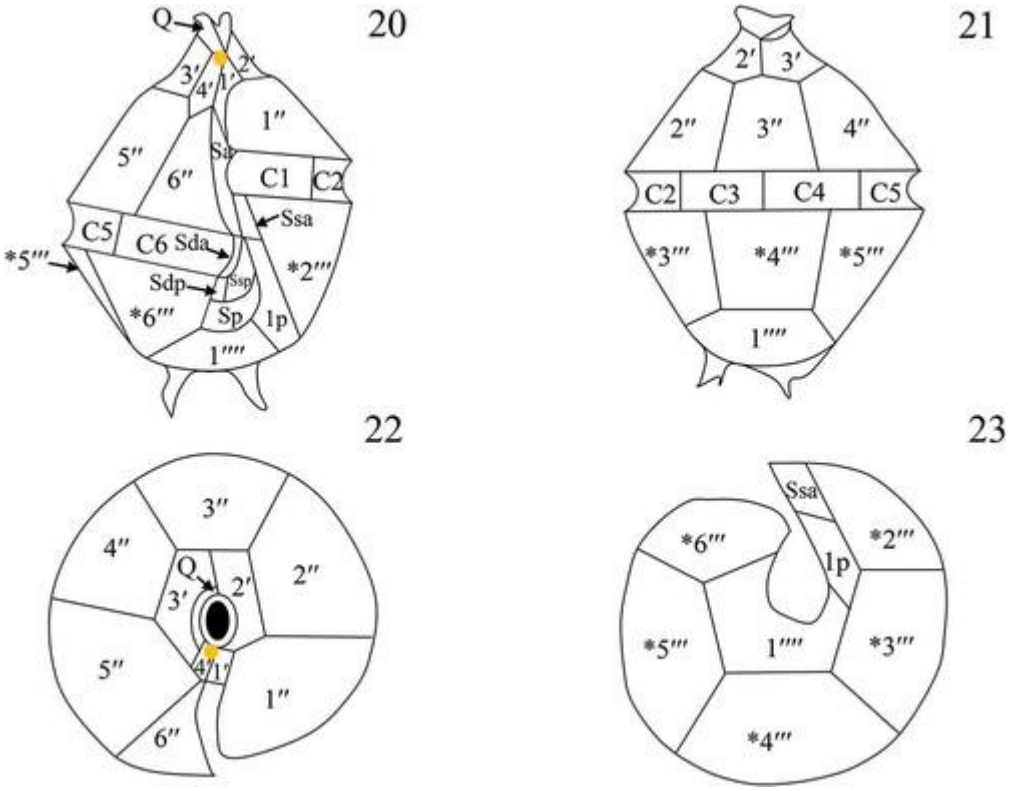

Figs 24–29. *Spiniferites* cf. *bentorii* from Bohai Sea, China, LM and SEM. Scale bars = 10 μm.

Fig. 24. Mid focus of a living cyst showing the apical boss (arrow) (LM).

Fig. 25. Mid focus of an empty cyst showing the intergonal processes (arrows) (LM).

Fig. 26. Ventral view of an empty cyst (SEM).

Fig. 27. Detail of the sulcus showing anterior sulcal plate (Sa) and posterior sulcal plate (Sp) (SEM).

Fig. 28. Apical view of an empty cyst showing the archeopyle (SEM).

Fig. 29. Apical-ventral view of an empty cyst showing the first and fourth apical plates (SEM).

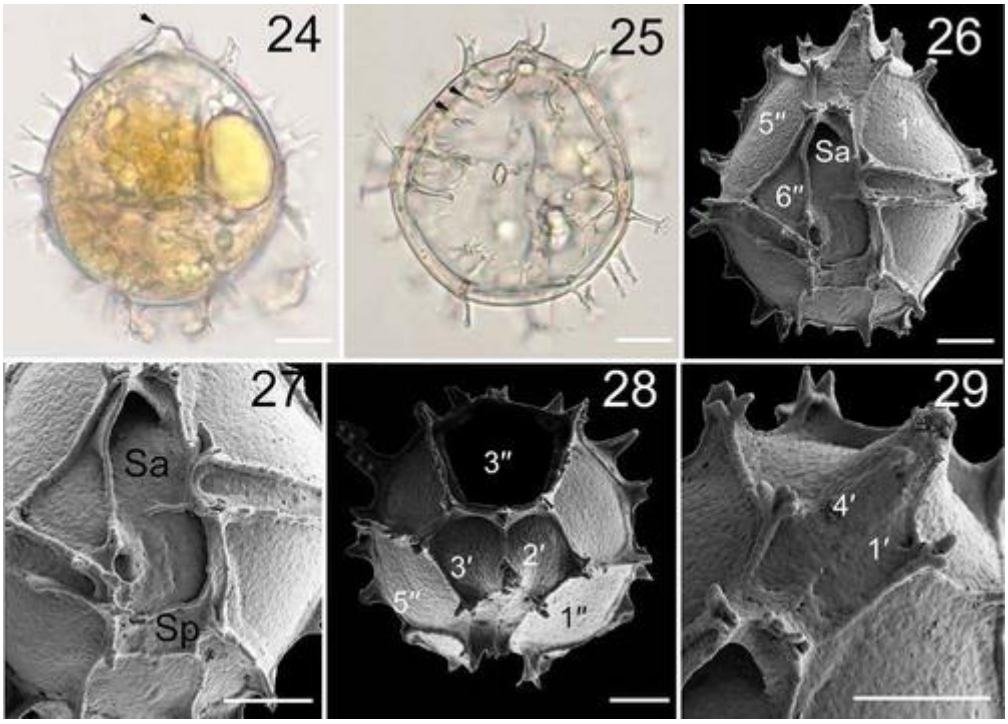

Figs 30–35. *Spiniferites hyperacanthus* from the East China Sea, LM and SEM. Scale bars = 10 μm.

Fig. 30. High focus of an empty cyst that originated strain TIO712, showing gonal (arrow) and intergonal (arrowhead) processes (LM).

Fig. 31. High focus of the same cyst shown in Fig. 30, showing gonal (arrow) and intergonal (arrowhead) processes and the reduced archeopyle (LM).

Fig. 32. Mid focus of the same cyst shown in Fig. 30, showing gonal (arrow) and intergonal (arrowhead) processes (LM).

Figs 33, 34. Dorsal view of cysts produced in culture of strain TIO260, showing the archeopyle (arrowheads) and the fenestrations at the base of processes (arrows) (SEM).

Fig. 35. Antapical view of a cyst produced in culture of strain TIO260, showing the intergonal process (arrow) (SEM).

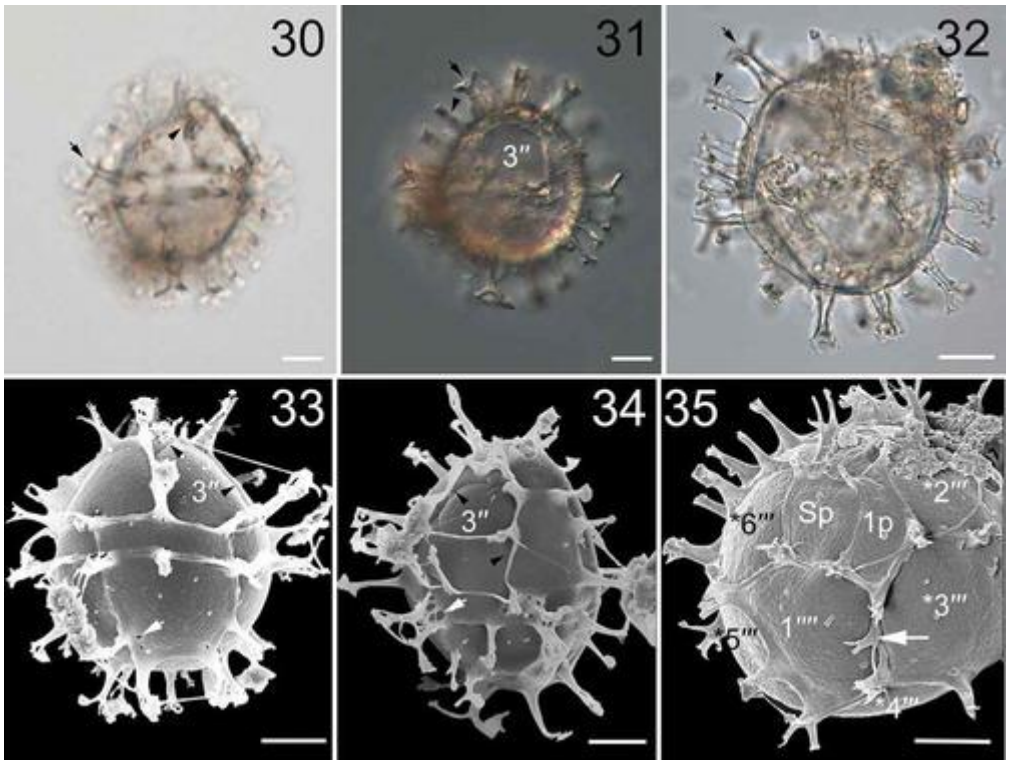

Figs 36–44. *Spiniferites hyperacanthus* strain TIO712 from the East China Sea, LM and SEM. Scale bars = 10 μm.

Fig. 36. High focus of a living cell showing the cingulum displacement (LM).

Fig. 37. Mid focus of a living cell showing the nucleus (N) (LM).

Fig. 38. Ventral view of a cell showing the two unequal antapical spines (SEM).

Fig. 39. Dorsal view of a cell showing the dextral torsion (SEM).

Figs. 40, 41. Ventral view of a cell showing the first and fourth apical plates (1′, 4′), a ventral pore (arrow), the quadrangular sixth precingular plate (6″) and the anterior sulcal plate (Sa) (SEM).

Fig. 42. Apical view of a cell showing four apical plates (1′–4′), Q plate and six precingular plates (1″–6″) (SEM).

Fig. 43. Antapical view of a cell showing five postcingular plates (*2‴–*6‴), one antapical plate (1⁗) and one posterior intercalary plate (1p) (SEM).

Fig. 44. The sulcus showing the anterior sulcal plate (Sa), anterior left sulcal plate (Ssa), posterior left sulcal plate (Ssp), anterior right sulcal plate (Sda), posterior right sulcal plate (Sdp) and posterior sulcal plate (Sp) (SEM).

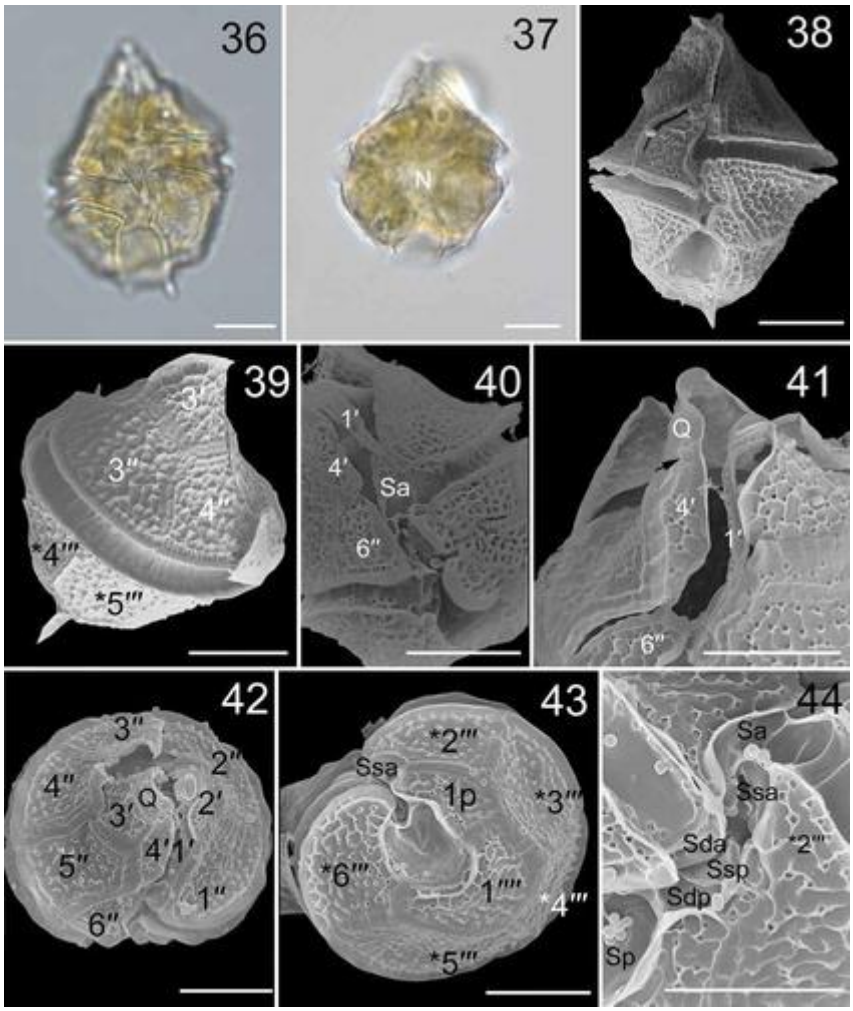

Figs 45–50. *Spiniferites lazus* from Baie de Vilaine, France, and *Spiniferites mirabilis* from the Gulf of California, LM. Scale bars = 10 μm.

Fig. 45. Mid focus of an empty cyst of *S. lazus* showing the archeopyle.

Fig. 46. High focus of an empty cyst of *S. lazus* showing two more developed antapical processes.

Fig. 47. High focus of an empty cyst of *S. lazus* showing the cingulum displacement.

Fig. 48. Mid focus of an empty cyst of *S. mirabilis* showing the antapical flange.

Fig. 49. High focus of an empty cyst of *S. mirabilis* showing cingulum displacement (arrows).

Fig. 50. High focus of an empty cyst of *S. mirabilis* showing the reduced archeopyle.

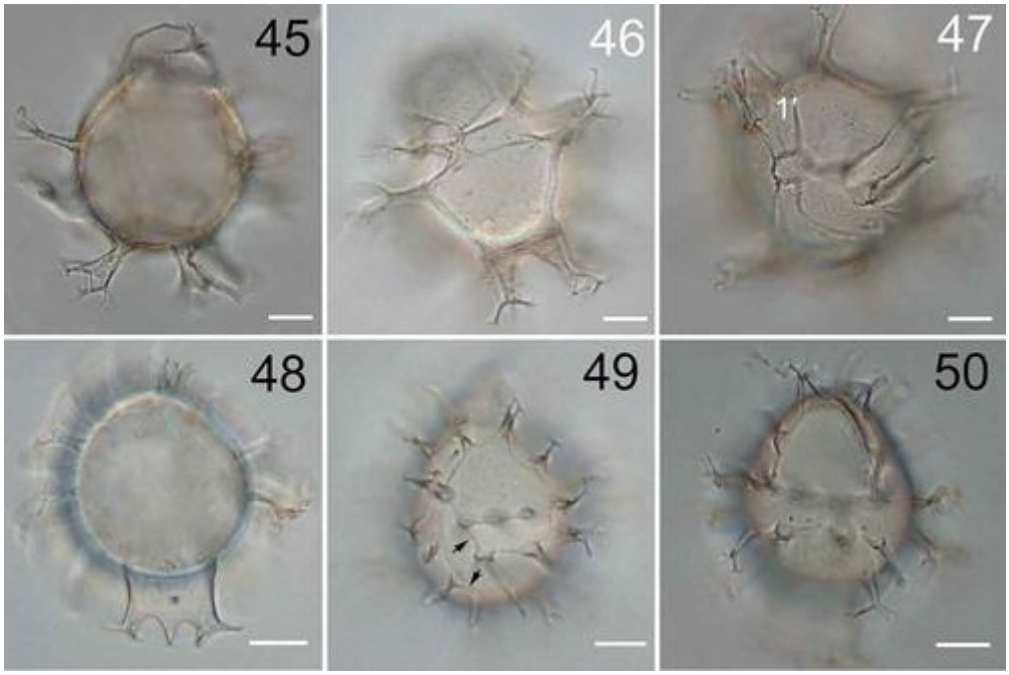

Figs 51–56. *Spiniferites ramosus* from the Canadian Pacific, LM and SEM. Scale bars = 10 μm.

Fig. 51. High focus of an empty cyst from which strain TIO904 was established, showing gonal processes (arrow) (LM).

Fig. 52. A living cyst produced in culture of strain TIO700, showing two red bodies (LM).

Fig. 53. Ventral view of a cyst produced in culture of strain TIO1400 (SEM).

Fig. 54. Apical view of a cyst produced in culture of strain TIO1400 (SEM).

Fig. 55. Dorso-antapical view of a cyst produced in culture of strain TIO1400 (SEM).

Fig. 56. A cyst produced in culture of strain TIO1400, showing the reduced archeopyle (SEM).

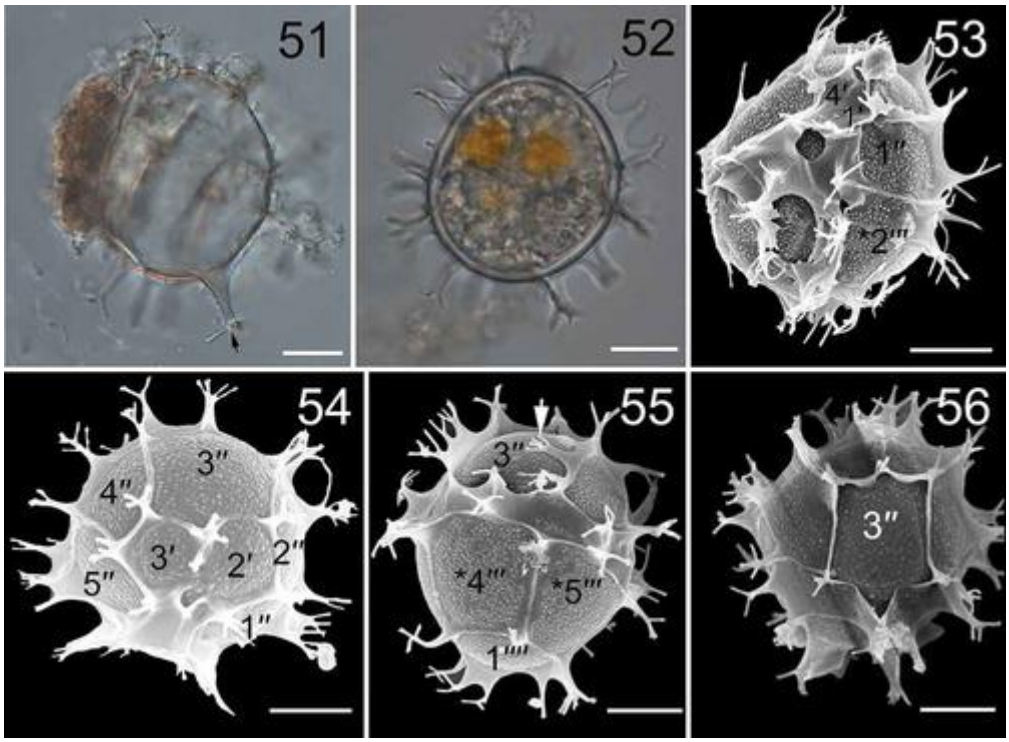

Figs 57–64. *Spiniferites ramosus* strain TIO701 from the Canadian Pacific, LM and SEM. Scale bars = 10 μm.

Fig. 57. High focus of a living cell showing cingulum displacement (LM).

Fig. 58. Mid focus of a living cell showing the nucleus (N) (LM).

Fig. 59. Ventral view of a cell showing the two equal antapical spines (SEM).

Fig. 60. Dorsal view of a cell showing neutral torsion (SEM).

Fig. 61. Apical-dorsal view of a cell showing two apical plates and four precingular plates (SEM).

Fig. 62. The sulcus showing the anterior sulcal plate (Sa), anterior left sulcal plate (Ssa), posterior left sulcal plate (Ssp), anterior right sulcal plate (Sda), posterior right sulcal plate (Sdp) and posterior sulcal plate (Sp) (SEM).

Fig. 63. Apical-ventral view of a cell showing the ventral pore (arrow) at the junction of plates 4′ and Q (SEM).

Fig. 64. Antapical view of a cell showing five postcingular plates, one antapical plate and one posterior intercalary plate (SEM).

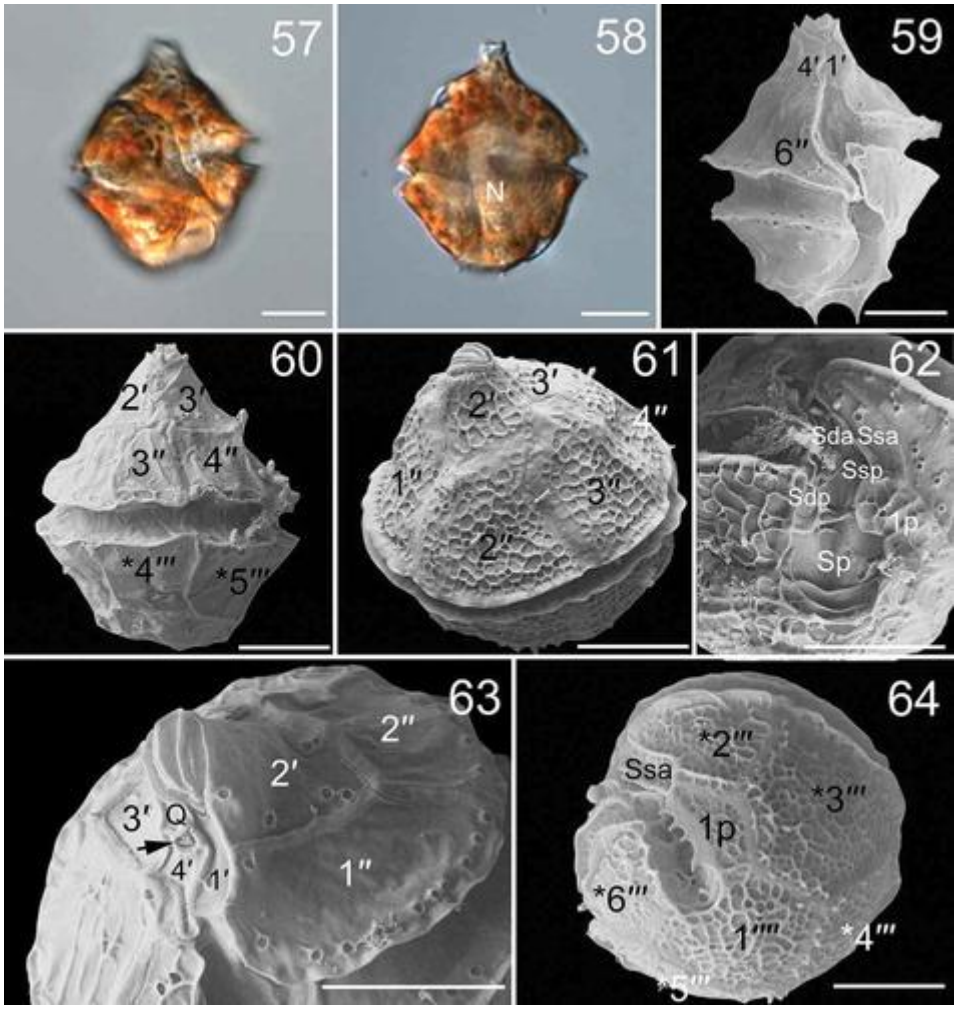

Figs 65–73. *Spiniferites scabratus* strain TIO706 from the Mediterranean Sea, LM and SEM. Scale bars = 10 μm.

Fig. 65. Mid focus of the empty cyst from which strain TIO706 was established (LM).

Fig. 66. High focus of the same cyst shown in Fig. 65, with the archeopyle and bifurcate tips of processes (arrow) (LM).

Fig. 67. High focus of the same cyst shown in Fig. 65, showing the granular surface (LM).

Fig. 68. Mid focus of a living cell showing the nucleus (N) (LM).

Fig. 69. High focus of a theca showing plates 1′, 4′ and 6″ (LM).

Fig. 70. Ventral view of a cell showing two equal antapical spines (arrows) (SEM).

Fig. 71. Dorsal view of a cell showing neutral torsion (SEM).

Fig. 72. Apical view of a cell showing plates 1′, 4′ and Q without a ventral pore (SEM).

Fig. 73. Antapical view of a cell showing three postcingular plates, one antapical plate and one posterior intercalary plate (SEM).

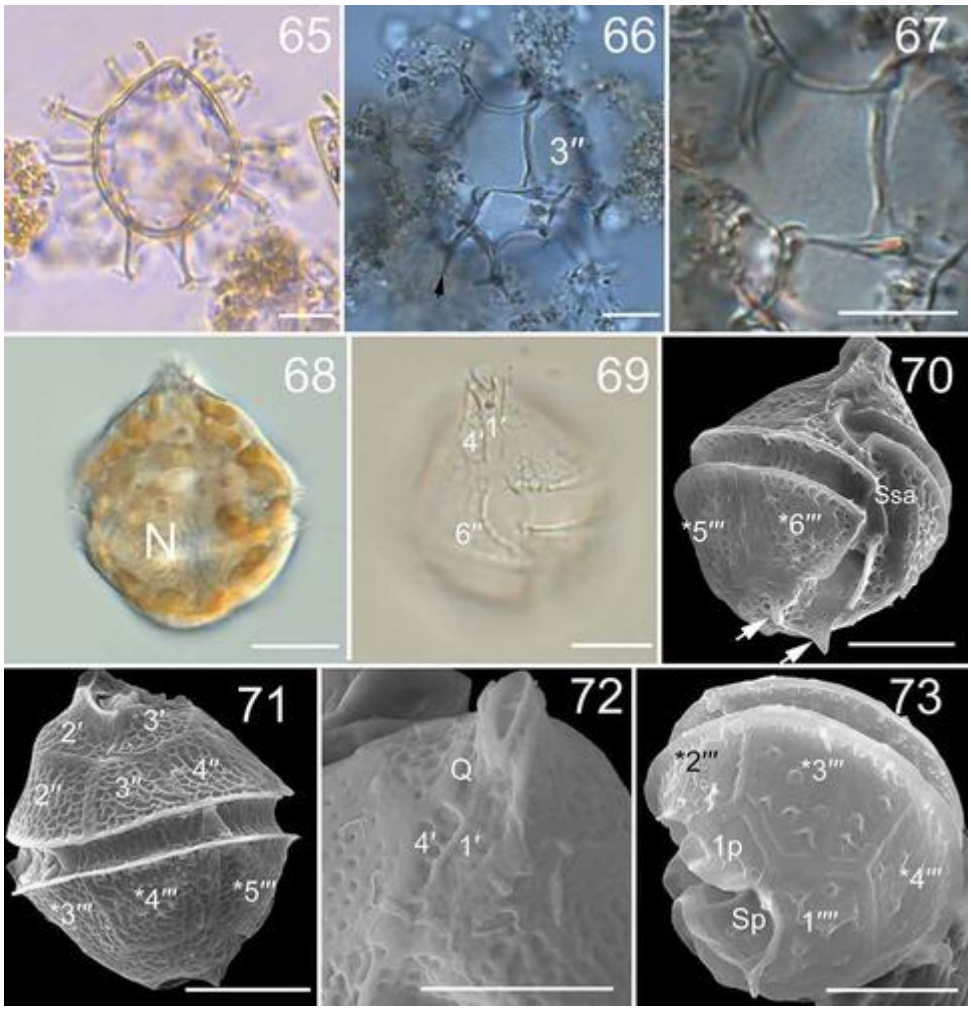

Figs 74–76. *Tectatodinium pellitum* from Gulf of California, LM. Scale bars = 10 μm.

Fig. 74. Mid focus of the empty cyst showing an apical protuberance (arrow) and two walls (arrowheads).

Fig. 75. High focus of the empty cyst showing the archeopyle.

Fig. 76. High focus of the empty cyst showing the spongy wall (arrow).

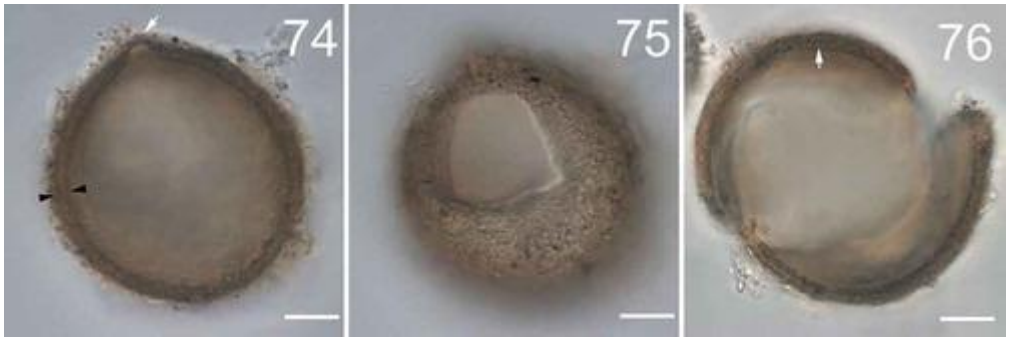

Fig. 77. Phylogeny of *Spiniferites* and *Tectatodinium* inferred from partial LSU rRNA gene sequences using Bayesian inference (BI). New sequences indicated in bold. Five families labelled and marked with vertical lines on the right. Branch lengths drawn to scale, with scale bar indicating number of nucleotide substitutions per site. Numbers on branches are statistical support values to clusters on the right of them (left: Bayesian posterior probabilities; right: maximum likelihood (ML) bootstrap support values). Only Bayesian posterior probabilities above 0.9 and ML bootstrap support values above 50 are shown. * indicates maximal support (BI posterior probability: 1.0, ML bootstrap support: 100).

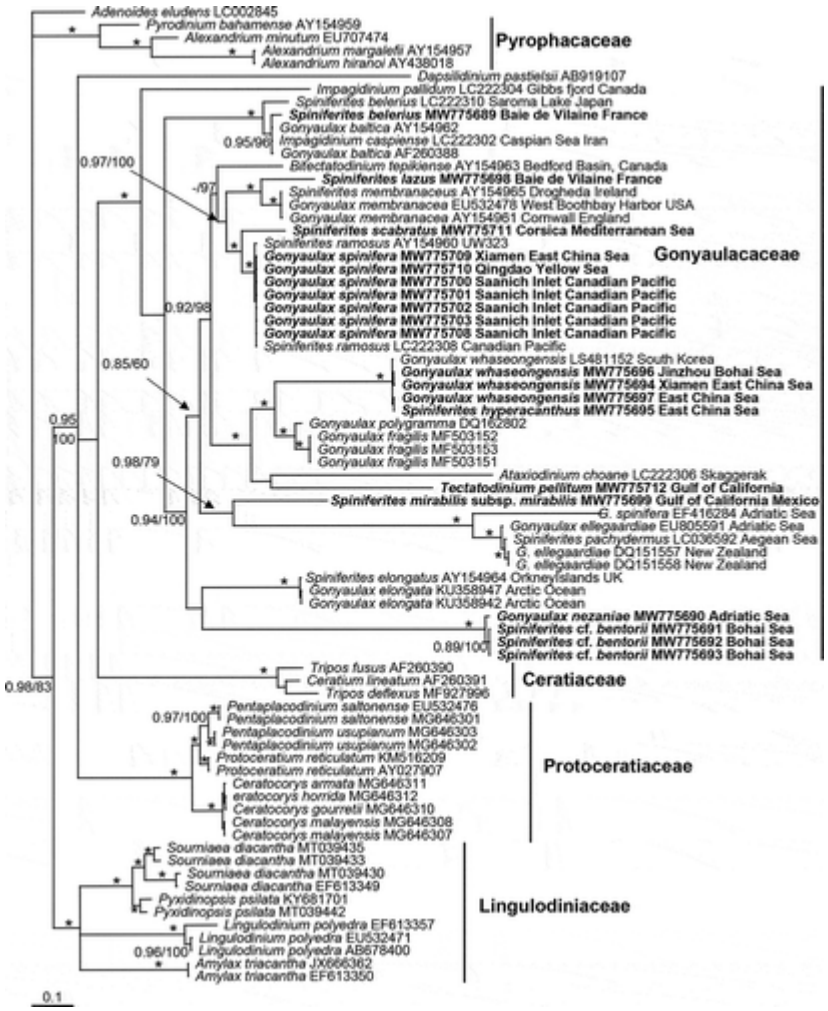

Fig. 78. Phylogeny of *Spiniferites* and *Tectatodinium* inferred from SSU rRNA gene sequences using Bayesian inference (BI). New sequences indicated in bold. Five families labelled and marked with vertical lines on the right. Branch lengths drawn to scale, with scale bar indicating number of nucleotide substitutions per site. Numbers on branches are statistical support values to clusters on the right of them (left: Bayesian posterior probabilities; right: maximum likelihood (ML) bootstrap support values). Only Bayesian posterior probabilities above 0.9 and ML bootstrap support values above 50 are shown. * indicates maximal support (BI posterior probability: 1.0, ML bootstrap support: 100).

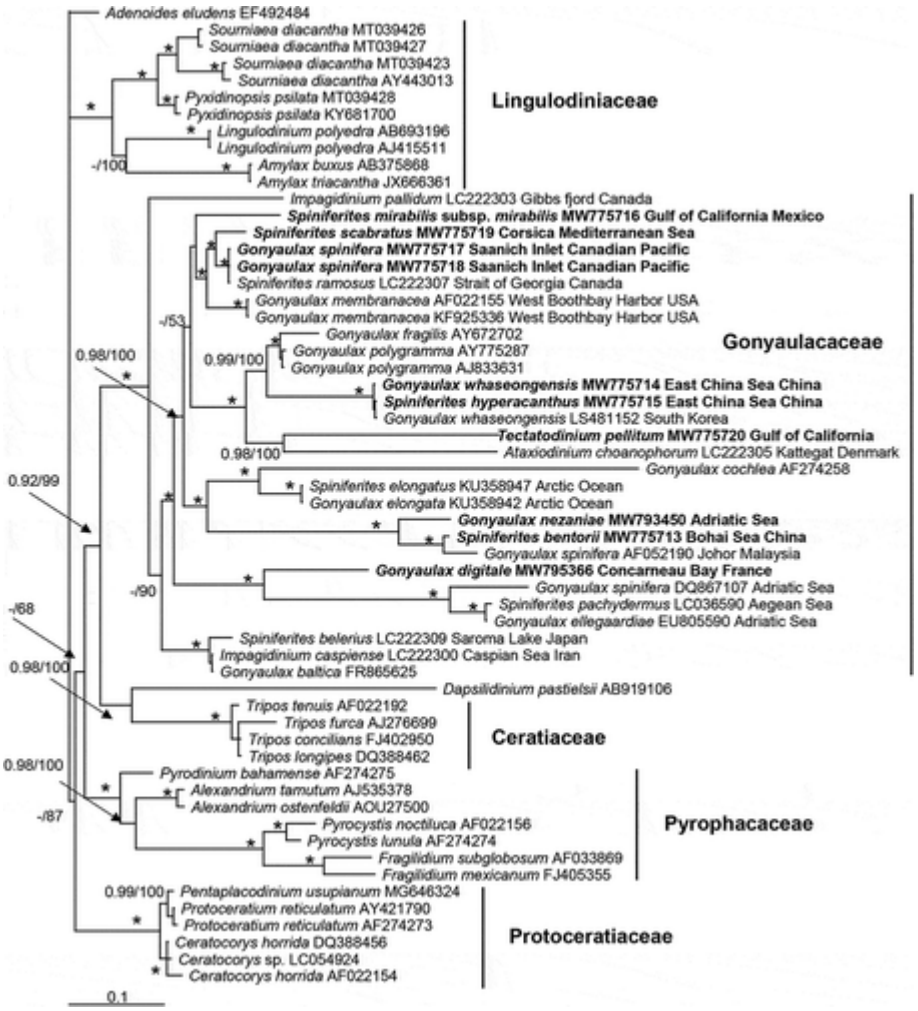
Adenoides eludens EF492484
Soumiaea diacantha MT039426
Soumiaea diacantha MT039427
Soumiaea diacantha MT039423
Soumiaea diacantha AY443013
Pyxidinopsis psilata MT039428
Pyxidinopsis psilata KY681700
Lingulodinium polyedra AB693196
Lingulodinium polyedra AJ415511
Amylax buxus AB375868
Amylax triacantha JX666361
Lingulodiniaceae
Impagidinium pallidum LC222303 Gibbs fjord Canada
Spiniferites mirabilis subsp. mirabilis MW775716 Gulf of California Mexico
Spiniferites scabratus MW775719 Corsica Mediterranean Sea
Gonyaulax spinifera MW775717 Saanich Inlet Canadian Pacific
Gonyaulax spinifera MW775718 Saanich Inlet Canadian Pacific
Spiniferites ramosus LC222307 Strait of Georgia Canada
Gonyaulax membranacea AF022155 West Boothbay Harbor USA
Gonyaulax membranacea KF925336 West Boothbay Harbor USA
Gonyaulax fragilis AY672702
Gonyaulax polygramma AY775287
Gonyaulax polygramma AJ833631
Gonyaulacaceae
Gonyaulax whaseongensis MW775714 East China Sea China
Spiniferites hyperacanthus MW775715 East China Sea China
Gonyaulax whaseongensis LS481152 South Korea
Tectatodinium pellitum MW775720 Gulf of California
Ataxiodinium choanophorum LC222305 Kattegat Denmark
Gonyaulax cochlea AF274258
Spiniferites elongatus KU358947 Arctic Ocean
Gonyaulax elongata KU358942 Arctic Ocean
Gonyaulax nezaniae MW793450 Adriatic Sea
Spiniferites bentorii MW775713 Bohai Sea China
Gonyaulax spinifera AF052190 Johor Malaysia
Gonyaulax digitale MW795366 Concarneau Bay France
Gonyaulax spinifera DQ867107 Adriatic Sea
Spiniferites pachydermus LC036590 Aegean Sea
Gonyaulax ellegaardiae EU805590 Adriatic Sea
Spiniferites belerius LC222309 Saroma Lake Japan
Impagidinium caspiense LC222300 Caspian Sea Iran
Gonyaulax baltica FR865625
Dapsilidinium pastielsii AB919106
Tripos tenuis AF022192
Tripos furca AJ276699
Tripos concilians FJ402950
Tripos longipes DQ388462
Ceratiaceae
Pyrodinium bahamense AF274275
Alexandrium tamutum AJ535378
Alexandrium ostenfeldii AOU27500
Pyrocystis noctiluca AF022156
Pyrocystis lunula AF274274
Fragilidium subglobosum AF033869
Fragilidium mexicanum FJ405355
Pyrophacaceae
Pentapiacodinium usupianum MG646324
Protoceratium reticulatum AY421790
Protoceratium reticulatum AF274273
Ceratocorys horrida DQ388456
Ceratocorys sp. LC054924
Ceratocorys horrida AF022154
Protoceratiaceae
-/100
-/53
0.98/100
0.99/100
0.98/100
0.92/99
-/90
-/68
0.98/100
0.98/100
-/87
0.99/100
0.1

Table 1. Information on *Spiniferites* and *Tectatodinium* strains or isolates used in this study. Species designation, strain/isolate identification, origin, collection date, GenBank accession numbers and yessotoxin (YTX). NA: not available.

Species	Strains/isolates	Collection date	Location	Latitude
S. belerius	-/18-896	27 July 2018	Baie de Vilaine, France	2°39.40′ N
S. bentorii	Pantan/-	04 May 2017	Pantan, Croatia (Mediterranean)	43°31.26′ N
S. bentorii	-/HSN114	04 Nov. 2020	Bohai Sea, China	38°29.51′ N
S. cf. *bentorii*	-/WN20	08 Mar. 2016	Panjin, Bohai Sea, China	42° 34.85′ N
S. cf. *bentorii*	-/WN21	08 Mar. 2016	Panjin, Bohai Sea, China	42° 34.85′ N
S. cf. *bentorii*	-/WN22	08 Mar. 2016	Panjin, Bohai Sea, China	42° 34.85′ N
S. hyperacanthus	TIO712/-	27 Feb. 2018	Xiamen Bay, East China Sea, China	24°35.568′ N

S. hyperacanthus	TIO260/-	31 Mar. 2016	Taiwan Strait, China	24°39.60′ N
S. hyperacanthus	GSJZ01/-	28 Apr. 2011	Jinzhou, Bohai Sea, China	40°43.60′ N
S. hyperacanthus	TIO1416/-	13 Oct. 2019	Sanmen, East China Sea, China	29°0.16′ N
S. lazus	-/18-898	27 July 2018	Baie de Vilaine, France	2°39.40′ N
S. mirabilis	-/20-188	13 Apr. 2014	Bahía de la Paz, Gulf of California	24° 52.54′ N
S. ramosus	TIO700/-	05 Mar. 2017	Saanich Inlet, Canada	48°39.30′ N
S. ramosus	TIO701/-	05 Mar. 2017	Saanich Inlet, Canada	48° 39.30′ N
S. ramosus	TIO702/-	05 Mar. 2017	Saanich Inlet, Canada	48° 39.30′ N

S. ramosus	TIO703/-	05 Mar. 2017	Saanich Inlet, Canada	48° 39.30′ N
S. ramosus	TIO704/-	05 Mar. 2017	Saanich Inlet, Canada	48° 39.30′ N
S. ramosus	TIO705/-	05 Mar. 2017	Saanich Inlet, Canada	48° 39.30′ N
S. ramosus	TIO904/-	05 Mar. 2017	Saanich Inlet, Canada	48° 39.30′ N
S. ramosus	TIO905/-	05 Mar. 2017	Saanich Inlet, Canada	48° 39.30′ N
S. ramosus	TIO1400/-	05 Mar. 2017	Saanich Inlet, Canada	48°40.23′ N
S. ramosus	-/WYJ	13 Nov. 2017	Xiamen Bay, East China Sea, China	24°35.57′ N
S. ramosus	TIO1218/-	12 Sep. 2019	Jiaozhou Bay, Qingdao, China	36°0.15′ N
S. scabratus	TIO706/-	18 Jan. 2016	Diane Lagoon, Corsica, France (Mediterranean)	42° 7.66′ N

T. pellitum	-/20-179	13 Apr. 2014	Bahía de la Paz, Gulf of California	24°52.54′ N

Table 2. Limit of detection (LoD) of yessotoxin in motile cells of *Gonyaulax spinifera* and *G. whaseongensis*. EV: extraction volume.

Species	Strain	Cell count	EV (µL)	LoD (fg cell^{-1})
Gonyaulax spinifera	TIO904	6300000	250	0.10
G. spinifera	TIO700	378000	200	7.22
G. spinifera	TIO701	1000000	200	2.73
G. spinifera	TIO704	830000	200	3.29
G. spinifera	TIO705	250000	200	10.91
G. whaseongensis	TIO260	324000	150	6.94
G. whaseongensis	TIO712	434000	250	1.44

Table 3. Comparisons of motile cell features of *Gonyaulax digitalis*, *Gonyaulax nezaniae* and *Bitectadinium tepikiense*

Character	*Gonyaulax digitalis sensu stricto*	*Gonyaulax nezaniae*	Motile cells of *Bitectadinium tepikiense*
Length	52.6 µm	37–68 µm	40–63 µm
Width	49.7 µm	33–52 µm	26–43 µm
Width of girdle	4.5 µm	3 µm	3–5 µm
Girdle displacement	?	3.0	2
Girdle overhang	?	1.7	0.5–1.5

Angle	?	20°	10–19°
Shape of 6″	?	Approx. equal sides	Approx. equal sides
Antapical spines	2	2(3)	2(3)
Length of spines	4.3–5.4 µm	2–11 µm	1–8 µm
Form of sulcus	?	Abruptly widened	Not abruptly widened
Apical horn	Prominent, 2 girdle widths in length	Prominent, 1.3–2 girdle widths in length	Prominent, 2–4 girdle widths in length
4′	?	Not separated	Not separated
References	This study	This study	Lewis *et al*. 2001

Table 4. List of currently inferred cyst-theca relationships of *Spiniferites* and related species.

Cyst	Motile stage	References
Spiniferites bentorii	*Gonyaulax nezaniae*	This study
Spiniferites bulloideus	*Gonyaulax baltica*	Ellegaard *et al.* 2002
Spiniferites elongatus	*Gonyaulax elongata*	Ellegaard *et al.* 2003
Spiniferites hyperacanthus	*Gonyaulax whaseongensis*	This study
Spiniferites membranaceus	*Gonyaulax membranacea*	Ellegaard *et al.* 2003
Spiniferites pachydermus	*Gonyaulax ellegaardiae*	Mertens *et al.* 2015
Spiniferites ramosus	*Gonyaulax spinifera*	Ellegaard *et al.* 2003; this study

Spiniferites scabratus	*Gonyaulax* cf. *spinifera*	This study
Bitectatodinium tepikiense	*Gonyaulax* cf. *digitalis*	Lewis *et al.* 2001
Impagidinium caspienense	*Gonyaulax baltica*	Mertens *et al.* 2018a

SUPPLEMENTARY INFORMATION

Figs S1–S2. *Gonyaulax digitalis* and *Spiniferites bentorii*-like cysts, LM. Scale bars = 20 μm.

Fig. S1. Living cell of *Gonyaulax digitalis* from Concarneau Bay, France.

Fig. S2. The living *Spiniferites bentorii*-like cyst (isolate HSN114) from Bohai Sea, China.